Soft Matter

Theory of colloid depletion stabilization by unattached and adsorbed polymers

Journal:	*Soft Matter*
Manuscript ID:	SM-ART-06-2015-001365.R2
Article Type:	Paper
Date Submitted by the Author:	01-Sep-2015
Complete List of Authors:	Semenov, Alexander; Insitut Charles Sadron, Shvets, Alex; Rice University,

Theory of colloid depletion stabilization by unattached and adsorbed polymers

A.N.Semenov *, **A.A.Shvets** †
Institut Charles Sadron, CNRS - UPR 22, Université de Strasbourg,
23 rue du Loess, BP 84047, 67034 Strasbourg Cedex 2, France
(September 1, 2015)

The polymer-induced forces between colloidal particles in a semidilute or concentrated polymer solution are considered theoretically. The study is focussed on the case of partially adsorbing colloidal surfaces involving some attractive centers able to trap polymer segments. In the presence of free polymer the particles are covered by self-assembled fluffy layers whose structure is elucidated. It is shown that the free-polymer-induced interaction between the particles is repulsive at distances exceeding the polymer correlation length, and that this depletion repulsion can be strongly enhanced due to the presence of fluffy layers. This enhanced depletion stabilization mechanism (which works in tandem with a more short-range steric repulsion of fluffy layers) can serve on its own to stabilize colloidal dispersions. More generally, we identify three main polymer-induced interaction mechanisms: depletion repulsion, depletion attraction, and steric repulsion. Their competition is analyzed both numerically and analytically based on an asymptotically rigorous mean-field theory. It is shown that colloid stabilization can be achieved by simply increasing the molecular weight of polymer additive, or by changing its concentration.

*To whom correspondence should be addressed.
†Current address: Department of Chemistry, Rice University, Houston, Texas, 77005, USA.

1. Introduction

Stabilization of colloidal dispersions is indispensable for numerous technological, industrial, biological and biomedical applications. [1,2] In many systems (including biological colloids [3–5]) colloidal particles are mixed with polymers that can significantly affect the colloidal stability. [1]

It is well-known that addition of a small amount of non-adsorbing polymer normally serves to destabilize a colloidal system due to the depletion flocculation effect. [1,2] A destabilization is also often observed in the case of reversible physical adsorption of added polymer onto the colloidal surfaces. [6,7] This effect is attributed to formation of polymer bridges between the particles. [8–11]

It was reported, however, that the depletion attraction can be suppressed by increasing the concentration of unattached polymer [1]. Higher concentrations of added polymer can impart colloidal stability also in the case of moderate attraction of polymer segments to colloidal particles. [12]

A number of theoretical approaches had been devised to explain the depletion *stabilization* effect [1,13]. However, most of these theories can be viewed as semiempirical in nature (see refs. [14,13] and references therein). [1]

A recently developed rigorous approach [13,14] attributes the free polymer induced (FPI) repulsion mostly to the entropic effect of polymer chain ends [16,14,13]. Interestingly, this effect is associated with the development of the polymer concentration maximum next to the depletion zone. [13,16,17]

It was shown [13] that the FPI repulsion in the semidilute or concentrated polymer regime can serve to kinetically stabilize colloidal systems. However, it is generally not strong enough (apart from some special cases) to impart the colloidal stability on its own in the case of non-adsorbing solid surfaces. Thus, the FPI interactions can be used to stabilize colloidal systems in combination with other stabilization mechanisms. This conclusion is drawn not only for non-adsorbing polymers [13], but also in the case of reversible adsorption of polymer chains on the colloidal particles [18].

Nevertheless, recent experimental results on metal nanoparticles [19,20] apparently indicate that the FPI repulsion can strongly enhance the colloidal stability, and even can provide a stabilization working alone (for particle size $\geq$ 30nm). The theory presented in this paper provides an explanation of the enhanced FPI stabilization effect. The model considered implies the presence of strongly adsorbing sites (centres) or their clusters on the colloidal particles (like the exposed patches of metal or citrate in the case of gold nanoparticles [21]). This should lead to a partial adsorption of some polymer segments located near the surface by binding to the attractive sites. We show that the emerging self-assembled adsorbed layers strongly can enhance the magnitude of the FPI repulsion even if the fraction of adsorbing sites is small.

The advantages of this colloidal stabilization method (as compared to the classical steric stabilization) is that polymer is an additive whose concentration and molecular weight can be rather easily varied to tune the interaction in a desired way. In addition, a rather dilute adsorbed layer does not block the colloidal surface leaving it accessible for other molecules.

The paper is organized as follows: The physical model is described in the next section; the structure of the fluffy adsorbed layer is also elucidated there. The basic theory of FPI interaction at low density of attractive centres is presented in section 3. The theory is then generalized to systems where the adsorbed and free chains have different molecular weights, and their effect on the FPI interactions is analyzed in section 4. Section 5 is devoted to the numerical results on depletion interactions at a relatively high density of adsorbing surface sites. In the next section 6 the calculated FPI interaction potentials are applied to analyze the forces between spherical particles (including the effects of the van der Waals and short-range depletion attractions). The main results are discussed and summarized in the last section.

---

[1] In many cases the polymer coils were regarded as ideal flexible chains, or as hard or soft (penetrable) spheres. [15]

2. The physical model and the adsorbed layer: structure and kinetics

2.1. Polymer near a solid wall

Let us consider a solution of homopolymer chains, with N units per chain, statistical segment length a_s and bulk monomer concentration c_b (corresponding to volume fraction $\phi_b = v_1 c_b$, where v_1 is the monomer volume) in the presence of a flat solid wall. The bulk solution is characterized by the correlation length ξ which depends on concentration:

$$\xi \simeq a/\sqrt{2v^* c_b}, \quad \phi_b \ll 1; \quad \xi \sim a, \quad \phi_b \sim 1 \tag{1}$$

where $a \equiv a_s/\sqrt{6}$, $v^* = \frac{1}{k_B T}\frac{\partial \mu_{int}}{\partial c_b}$ is the effective monomer virial parameter, and μ_{int} is the osmotic contribution to the monomer chemical potential. [13] In the second virial approximation $\mu_{int}(c_b) \simeq k_B T v c_b$, where v is the second virial coefficient of monomer interactions (by monomers here we mean monomer residues, repeat units of the polymer chain).

In what follows we are mostly interested in the regime of short correlation length as compared to the polymer coil size: $\xi \ll R$, where $R = a\sqrt{N}$ is the gyration radius. We also assume the marginal solvent regime, $c_b \gg v/a_s^6$, with sufficiently long chains, $N \gg 1/(v^* c_b)$. [2] It is important to note that marginal solvent regime does not necessarily mean that the solution is close to the theta-conditions. Of course, close enough to the theta temperature the solvent is always marginal. However, the marginal solvent conditions are often realized for polymers in solvents that are normally considered by the experimentalists as pretty good (like polystryrene, PS, in toluene). Moreover, even athermal polymer systems (with no attraction between the chain segments, but only steric repulsion) can be in the marginal solvent conditions if the polymer chains are semiflexible since the ratio v/a_s^3 is always small in this case (a polymer is semiflexible if its persistence length is much longer than its effective chain diameter).

Let us clarify the point: by definition, the solvent is marginal if the chains are not swollen significantly even in the dilute regime (i.e., the chain statistics are nearly Gaussian). The swelling factor $\alpha = R/R_0$ (where R_0 is the ideal Gaussian chain size) is defined by the Fixman parameter [23–25]

$$z_F = \left(\frac{3}{2\pi}\right)^{3/2} \frac{vN^{1/2}}{a_s^3}$$

As a reasonable quantitative criterion of the marginal solvent regime one can demand that the degree of chain swelling is less than 20% ($\alpha < 1.2$) which corresponds to $z_F \lesssim 0.5$. [23–25] Using this criterion for example for PS in toluene ($a_s \approx 7.5\text{Å}$, $v \approx 40\text{Å}^3$) [26,27] we get $N \lesssim 300$. Therefore, the marginal solvent regime is always relevant for toluene solutions of PS with molecular weight $M \lesssim 30000$. It is also relevant for longer PS chains well in the semidilute regime, for concentrations $\gtrsim 0.1\,\text{g/cm}^3$.

Let us return to the polymer solution near a wall. The next question concerns the equilibrium monomer concentration profile near the wall, $c = c(x)$, where x is the distance to the surface. Obviously $c(\infty) = c_b$. The concentration at the surface, $c(0)$, depends on the polymer/wall interactions. Let us consider first the case of maximum bulk concentration $c_b = c_{max} = 1/v_1$ ($\phi_b = 1$) corresponding to a polymer melt. Due to the incompressibility of the melt, the surface effect is very local with microscopic range δ of the order of monomer size. Hence, the concentration profile is nearly uniform outside this thin surface layer: $c(x) \simeq c_b$ for $x > \delta$. The effects considered below correspond to much longer length scales on the order of the coil size $R \gg \delta$. The polymer chain statistics at these length-scales nearly does not depend on the local polymer/surface interactions, hence we can disregard the surface layer formally setting $\delta = 0$. In this sense we can also set $c(0) = c_b$ meaning that the surface effect is 'neutral' and arriving at the effective boundary condition on the surface of the Neumann type:

$$\frac{\mathrm{d}c}{\mathrm{d}x} = 0, \quad x = 0 \tag{2}$$

Within the mean field approach [13] this boundary condition together with the incompressibility ensure that the equilibrium mean-field molecular potential $U(x)$ is constant (for $x > \delta$).

---

[2] Shorter chains are not interesting as they are anyway not efficient for colloidal stabilization.

Indeed, defining $\psi(x,s)$ as the partition function of a chain of s units with one end at the distance x, and adopting the continuous Gaussian chain mean-field model, we can write the concentration profile as [23]:

$$c(x) = \frac{c_b}{N}\int \psi(x,s)\psi(x,N-s)\mathrm{d}s \tag{3}$$

In the presence of the molecular field $U(x)$ the function ψ satisfies the Edwards equation [22,23,13]:

$$\frac{\partial\psi(x)}{\partial s} = a^2\frac{\partial^2\psi(x)}{\partial x^2} - U(x)\psi(x) \tag{4}$$

with $\psi(x,0)=1$. [3] The condition (2) can be generally satisfied only if

$$\frac{\mathrm{d}\psi(x)}{\mathrm{d}x} = 0, \quad x = 0 \tag{5}$$

The above equations allow to find $c(x)$ for a given $U(x)$. The solution is particularly simple for $U(x) = \text{const}$: $c(x) \equiv c_b$. This result validates the assumption that $U(x) = \text{const}$.

For similar reasons the effective boundary condition (5) is also applicable to describe the polymer statistics in the case of concentrated or semidilute solution regime at length-scales exceeding the static correlation length ξ of polymer concentration fluctuations: in this regime as well $c(x) \simeq c_b$ and $U(x) \simeq \text{const}$ as long as we are not interested in the short-range details for $x \lesssim \xi$.

2.2. The effect of attractive sites

We now take into account the presence of sites that can strongly adsorb polymer segments on the surface. As a reference model we consider a basically neutral surface decorated with some randomly distributed attractive sites covering a small fraction of the surface. To simplify the model, we assume that a monomer unit can form a bond with just one attractive site on the surface (and vice versa). We consider such units as frozen and label them 'white'. All other monomers are 'black'. The irreversible adsorption can be then considered as a process of recoloring the polymer units from 'black' to 'white'.

In the simplest case, we postulate that 'black' units can instantly turn 'white' with probability $p(x)$. The function $p(x)$ is localized near the surface: $p(x) = 0$ for $x > \delta_b$, where δ_b is the bond size, so $\delta_b \sim a \ll R$. After the transformation the total number of 'white' units (per unit area) is

$$\sigma_a = c_b\int_0^{\delta_b} p(x)\mathrm{d}x \tag{6}$$

where σ_a is the surface concentration of the attractive sites. The chains with 'white' units are then considered as adsorbed, and the first quantity of interest is the concentration profile $c_a(x)$ of the adsorbed polymers. All other chains (with no 'white' units) are free, their concentration profile is $c_f(x)$.

To calculate $c_a(x)$ we note that, once the colors of the units are not distinguished, the statistical conformational distribution $Z[\Upsilon]$ of all chains must remain unchanged, $Z = Z_0[\Upsilon]$, where Υ is the set of coordinates of all units. Adding colors, we multiply Z_0 by the color factor:

$$Z[\Upsilon, col] = Z_0[\Upsilon]\, Z_{col} \tag{7}$$

where $Z_{col} = \prod_i w_i$ is the product of color weights for all units: $w_i = p(x)$ for a white unit i, and $w_i = 1 - p(x)$ for black units. Therefore $Z[\Upsilon, col]$ is the equilibrium distribution of the system of annealed chains whose units can independently choose from 2 states (black and white) in the external field $u_0(x)$ for black units and $u_1(x)$ for white units, such that $e^{-u_1(x)} = p(x)$, $e^{-u_0(x)} = 1 - p(x)$. Right after the instant coloring event the joint distribution is given by eq. (7), hence the distribution of free chains (with no white units) is consistent with the surface field

$$u_0(x) = -\ln\left(1 - p(x)\right) \tag{8}$$

[3] Here and below the thermal energy k_BT is considered as the energy unit.

In other words, the distribution of free (entirely black) chains is defined by eqs. (4), (5) with $U(x) = u_0(x)$. As the field $u_0(x)$ is localized, $\delta_b \ll R$, its effect can be replaced by the effective boundary condition (instead of eq. (5)):

$$\frac{\mathrm{d}\psi(x)}{\mathrm{d}x} = \frac{\psi(x)}{b}, \quad x = \delta_b \tag{9}$$

where the extrapolation length [4] b is defined by the potential $u_0(x)$:

$$b \simeq a^2 / \int p(x)\mathrm{d}x = a^2 c_b/\sigma_a \tag{10}$$

where eq. (6) is also used. [5]

For $x > \delta_b$ the Edwards equation then reduces to the ideal chain propagation ('free diffusion'): $\frac{\partial\psi}{\partial s} = a^2\frac{\partial^2\psi}{\partial x^2}$. This ideal chain problem was solved long ago [30,31]. The result depends on the parameter

$$\varkappa = R/b = \sqrt{N}\sigma_a/(ac_b) \tag{11}$$

which gives the reduced surface concentration of attractive sites. The free-chain partition function is

$$\psi(x,u) = 1 - \mathrm{erfc}\left(\frac{\bar{x}}{2\sqrt{u}}\right) + e^{\varkappa\bar{x}+u\varkappa^2}\,\mathrm{erfc}\left(\frac{\bar{x}}{2\sqrt{u}} + \varkappa\sqrt{u}\right)$$

where erfc is the complementary error function, $\bar{x} = x/R$, $u = s/N$. The concentration profile $c_f(x)$ for free chains is then defined in eq. (3). Recalling that the total concentration $c(x) = c_a(x) + c_f(x) = c_b$ is uniform (see the end of the previous section) we find the profile for adsorbed chains

$$c_a(x) \simeq c_b \int_0^1 [1 - \psi(x,u)\psi(x,1-u)]\,\mathrm{d}u \tag{12}$$

In particular,

$$c_a(0)/c_b \simeq \int_0^1 \left[1 - \mathrm{Fd}(\varkappa\sqrt{u})\mathrm{Fd}(\varkappa\sqrt{1-u})\right]\mathrm{d}u$$

where $\mathrm{Fd}(z) = \exp(z^2)\,\mathrm{erfc}(z)$. The surface concentration of adsorbed chains, $c_a(0)/c_b$, is shown in Fig. 1 as a function of $\varkappa$: $c_a(0)$ is small for $\varkappa \ll 1$ and it is close to c_b for $\varkappa \gg 1$ (adsorbed chains dominate near the surface):

$$c_a(0)/c_b \simeq \frac{8}{3\sqrt{\pi}}\varkappa, \quad \varkappa \ll 1; \qquad c_a(0)/c_b \simeq 1 - 1/\varkappa^2, \quad \varkappa \gg 1$$

Note that due to the large factor $\sqrt{N}$ in eq. (11), the regime $\varkappa \gtrsim 1$ can be realized even for a small surface concentration of adsorbing centers.

Let us consider the two asymptotic regimes in more detail. For $\varkappa \ll 1$ we obtain

$$c_a(x)/c_b \simeq \varkappa f_0\left(\frac{x}{R}\right), \quad f_0(\bar{x}) = \frac{8}{3\sqrt{\pi}}\left(1 + \frac{1}{4}\bar{x}^2\right)\exp\left(-\frac{1}{4}\bar{x}^2\right) - 2\bar{x}\left(1 + \frac{1}{6}\bar{x}^2\right)\mathrm{erfc}\left(\frac{\bar{x}}{2}\right) \tag{13}$$

The function $f_0(\bar{x})$ is displayed in Fig. 2. The total adsorbed mass is

$$\Gamma_a = \int_0^\infty c_a(x)\mathrm{d}x \simeq c_b\varkappa R = N\sigma_a \tag{14}$$

---

[4] The extrapolation length b is the distance between the physical surface ($x = \delta_b$) and the fictitious surface where the linearly extrapolated $\psi(x)$ should vanish. [28]

[5] It may seem that eq. (10) requires $u_0 \simeq p \ll 1$. However, this requirement is just an artifact of the continuous chain model, while eq. (10) is more general: it is always valid as long as $b \gg a$.

In the opposite regime, $\varkappa \gg 1$, the dependence on $\varkappa$ saturates:

$$c_a(x)/c_b \simeq f_1\left(\frac{x}{R}\right), \quad f_1(\bar{x}) = \int_0^1 \left[1 - \mathrm{erf}\left(\frac{\bar{x}}{2\sqrt{u}}\right) \mathrm{erf}\left(\frac{\bar{x}}{2\sqrt{1-u}}\right)\right] \mathrm{d}u \tag{15}$$

The reduced concentration profile in this case is also shown in Fig. 2. The total adsorbed amount,

$$\Gamma_a \simeq (2/\sqrt{\pi})\, c_b R \tag{16}$$

is now independent of the concentration of attractive sites.

Using equations (6) ($\sigma_a \sim c_b \delta_b p$) and (11) one finds $\varkappa \sim \sqrt{N} p \delta_b / a \sim \sqrt{N} p$. Therefore, the regime $\varkappa \gg 1$ can be naturally realized with $p \sim 1$ and $N \gg 1$: in this case $\varkappa \sim N^{1/2} \gg 1$. As a useful particular case we can assume that every chain unit in a surface layer of thickness δ_b is instantly turned to the bonded state (i.e., these units get instantly trapped by the surface attractive sites). By doing this we model surface/monomer interactions with the highest density of adsorbing sites. Therefore, the resultant adsorbed layers must correspond to the asymptotic regime $\varkappa \gg 1$. The concentration profiles, $c_a(x)$, have been calculated for different $\delta_b/R = 0.05,\ 0.2,\ 0.5$ directly using the SCFT approach (see ref. [13] for details) based on the Edwards equation (4) involving the potential field $U(x) = u_0(x)$ for the free (black) chains. The obtained profiles are identical in all the three cases provided that x is redefined as the distance to the δ_b-layer of the trapped (white) units, i.e. $x = -\delta_b$ corresponds to the solid surface (Fig. 2). Moreover, the SCFT profiles also coincide with the analytical prediction for $\varkappa \gg 1$, eq. (15) (see Fig. 2). Interestingly, the total number of adsorbed chains is $\mathfrak{N}_a = \frac{c_b}{N}(\Delta + \delta_b)$, where $\Delta = \frac{2}{\sqrt{\pi}} R$. The δ_b contribution is neglected in what follows since $\delta_b \ll R$.

Two remarks are due here. First, strictly speaking, the calculated profiles $c_f(x)$, $c_a(x)$ are valid right after the coloring instant. What if they change afterwards? The answer is: if the potential $u_0(x)$ is present, then the chain conformational distribution, eq. (7), is always at equilibrium, so it does not change in time. If the system is incompressible (say, in the melt case), the required molecular field $u_0(x)$, eq. (8), is created self-consistently (since the overall monomer density profile would be inhomogeneous for any other potential, leading to a violation of the incompressibility condition). In the case of a solution with a finite ξ, the concentration profile changes at $x \sim \xi$. However, the effective boundary condition (9) is still applicable at larger distances $x \gg \xi$ due to the repulsive molecular field $u(x)$ which develops self-consistently in the proximal zone $x \sim \xi$. The field $u(x)$ is associated with an elevated total monomer concentration in this zone: $u(x) \simeq v^* \delta c(x)$. The concentration increment $\delta c(x)$ is mainly due to adsorbed chains, $c_a(x)$, whose effect is reduced by a depletion of free chains near the surface. To keep the total c nearly constant we have to demand $\delta c \ll c_a$ for $x \gg \xi$, which gives, by virtue of the Edwards equation, the condition [6]

$$\frac{1}{a^2} \int_0^x v^* c_a(x) \mathrm{d}x \gg 1/\max(b, \xi) \ \text{ for } \ x \gg \xi \tag{17}$$

Using eqs. (13), (15) one can verify that the condition (17) is always true provided that $\xi \ll R$, i.e., in the semidilute or concentrated solution regimes. To resume, we find that the redistribution of segments of free (or adsorbed) chains after an instantaneous surface bond formation is a negligibly weak effect for $x \gg \xi$.

Another remark concerns the boundary condition. So far we assumed the neutral wall (Neumann) condition, eq. (5). We argued above that due to the virtual incompressibility of the system the true boundary condition is irrelevant for the free chain statistics at length scales $x \gg \xi$. However, the surface bond formation (coloring) happens at short distances $x \sim \delta_b \lesssim \xi$, hence this process may be affected by the polymer/wall interaction. However, the total number of adsorbed units (per unit area) must be equal to the number of traps ($= \sigma_a$) which is known (it is assumed that there are enough monomers in the δ_b−layer to saturate all traps, $\int_0^{\delta_b} c(x) \mathrm{d}x > \sigma_a$, since otherwise instantaneous coloring would not be possible). As was established before [32], it is the total number of units at the surface ($= \sigma_a$) that defines the concentration profiles at $x \gg \delta_b$, hence the

[6] The additional condition, $x \gg \xi$, is applied here since we are interested in the effect of the field $u_0(x)$ on the large-scale monomer distribution, i.e., for $x \gg \xi$. For the same reason we replace b with $\max(b, \xi)$: this change does not affect the conformational distribution of chain segments on the length-scales larger than ξ.

effective boundary condition (9) and eq. (10) for b stay essentially valid in the general case, for the arbitrary polymer/surface interaction (in particular, also when the surface with no attractive sites is purely repulsive).

Let us now lift the assumption of an instant surface bond formation: it could be unrealistic in the case of relatively strong bonds between polymer segments and colloidal surface. In this case, the bond formation may be delayed by rather high activation energy barriers [29] (note that the activation energy is relevant also for H-bonds; in the general case the barriers are related to the free energy involving both enthalpic and entropic contributions). To account for this effect below we consider a continuous adsorption process using the following reaction-controlled kinetic model: At any instant dt a black (free) unit can turn white (adsorbed) with probability $\mathrm{d}p = f\mathrm{d}t$, where the rate f depends only the position x of the unit (but not on positions or colors of any neighboring units). In the spirit of the mass action law the rate $f = f(x,t)$ can be factorized as $f(x,t) = k(x)\,(\sigma_a - \sigma(t))$, $k(x)$ is the rate constant localized at $x \sim \delta_b$, and $\sigma_a - \sigma$ is the current surface concentration of the active (unsaturated) attractive centres. In this process the probability $p = p(x,t)$ that a unit at the position x is immobilized (white) is always independent on the positions of other units, and the joint conformation/color distribution remains always equal to the annealed distribution, eq. (7), so that the black loops are always at equilibrium with the self-consistent molecular field $u_0(x,t) = -\ln(1-p(x,t))$. Hence no relaxation takes place between the coloring events. The time dependent fraction of immobilized units, $p = p(x,t)$, is defined by the master equation

$$\frac{\partial p}{\partial t} = k(x)\,(\sigma_a - \sigma(t))\,(1-p) \tag{18}$$

where

$$\sigma(t) = c_b \int_0^\infty p(x,t)\mathrm{d}x$$

Assuming $p \ll 1$ we get (integrating eq. (18)):

$$\mathrm{d}\sigma/\mathrm{d}t = K c_b(\sigma - \sigma_a), \quad K \equiv \int_0^\infty k(x)\mathrm{d}x$$

leading to

$$\sigma(t) = \sigma_a\left(1 - e^{-t/\tau}\right), \quad p(x,t) = \frac{\sigma(t)k(x)}{c_b K}$$

where $\tau = 1/(Kc_b)$ is the characteristic bond-formation time. Hence, for $t \gg \tau$ we have $\sigma \simeq \sigma_a$, and the joint conformation/color distribution becomes exactly the same as after the instant coloring event considered above. So, eq. (12) and other equations below it remain applicable after the bond-formation process. [7]

3. FPI interaction between parallel solid surfaces with attractive centres

The polymer/surface interactions considered in the previous section make sure that the polymer is partially adsorbed at the colloidal surface due to the presence of attractive sites there. The thickness of the adsorbed layer is always defined by the polymer coil size R. In what follows we assume that the colloidal particle size D_c is larger than the layer thickness, $D_c \gg R$. Then, by virtue of the Derjaguin approximation, the interaction of colloidal particles can be reduced to the interaction between parallel flat solid surfaces, that is to the case of a polymer solution in a slit pore $(0 < x < h)$.

In this section we focus on the regime $\varkappa \ll 1$ where the adsorbed layer is rather dilute: the free chains dominate by concentration everywhere, $c_a(x) \ll c_f(x) \sim c_b$. The profile $c_f(x)$ is thus only weakly inhomogeneous, so the molecular field $u = u(x)$ required to generate the inhomogeneity is also weak, $uN \ll 1$. The statistics of adsorbed chains is then basically not affected by the

[7] The condition $p \ll 1$, which is equivalent to $\sigma_a \ll c_b\delta_b$, is not necessary for this conclusion.

molecular field, and the effect of two confining surfaces ($x = 0$ and $x = h$) can be taken into account by the reflection principle [16,33,34] leading to a periodically extended concentration profile $c_a(x)$ (defining the monomer distribution of adsorbed chains):

$$c_a(x) = \sum_{n=-\infty}^{\infty} c_a^{(1)}(|x - nh|) \tag{19}$$

where $c_a^{(1)}(x)$ is the adsorbed concentration profile in the semi-space $x > 0$ next to a single solid surface at $x = 0$, as considered in the previous section. Note that the total amount of adsorbed polymer is fixed

$$\int_0^h c_a(x)\mathrm{d}x = 2\Gamma_a \simeq 2c_b \varkappa R$$

The total concentration is nearly constant and is equal to the bulk concentration c_b since we consider a semidilute of concentrated solution with $\xi \ll R$ (which is true for $c_b v^* N \gg 1$, see eq. (1)) and $h \gg \xi$:

$$c_f(x) + c_a(x) = c_b \tag{20}$$

(This condition may be violated at short h, the implications are considered in section 6.2.)

The grand thermodynamic potential Ω of the system (per unit area), is

$$\Omega\,[c] = \mathcal{F}\,[c] - \mu_b \int_0^h c\mathrm{d}x + \Pi_b h$$

where $\mathcal{F}\,[c]$ is the free energy, μ_b and Π_b are the monomer chemical potential and osmotic pressure in the bulk. The potential Ω includes the contribution Ω_{int} due to monomer interactions and the conformational term Ω_{conf} reflecting a depletion of the number of chain conformations in an inhomogeneous state (see ref. [13]): $\Omega = \Omega_{conf} + \Omega_{int}$,

$$\Omega_{conf}\,[c] = \mathcal{F}_{conf}\,[c] - \frac{1}{N}\ln\frac{c_b}{N}\int_0^h c\mathrm{d}x + \frac{c_b}{N}h \tag{21}$$

where $\mathcal{F}_{conf}\,[c]$ is the conformational free energy,

$$\Omega_{int}\,[c] = \int_0^h \left[f_{int}(c) - \mu_{int}(c_b)c + \Pi_{int}(c_b)\right]\mathrm{d}x \tag{22}$$

where $f_{int}(c)$ is the (osmotic) free energy density due to excluded-volume monomer interactions, and $\mu_{int}(c) = \partial f_{int}(c)/\partial c$, $\Pi_{int}(c) = c\mu_{int}(c) - f_{int}(c)$ are the corresponding parts of the local chemical potential and the local osmotic pressure. In the third virial approximation

$$f_{int}(c) \simeq vc^2/2 + wc^3/6 \tag{23}$$

$$\mu_{int}(c) \simeq vc + wc^2/2, \quad \Pi_{int}(c) \simeq vc^2/2 + wc^3/3$$

hence

$$\Omega_{int} \simeq \int_0^h (c - c_b)^2 \left[\frac{v}{2} + \frac{w}{6}(c + 2c_b)\right]\mathrm{d}x$$

Note now that $\Omega_{int} \simeq \mathrm{const} = 0$ due to the incompressibility, and the same is nearly true regarding the conformational contribution of adsorbed chains (which are dominated by the free chains). Therefore,

$$\Omega \simeq \mathrm{const} + \Omega_{conf}[c_f(x)]$$

i.e., we should focus on the conformational free energy of unattached chains which should be obtained as a function of h.

The general expression for $\mathcal{F}_{conf}$ (per unit area) in a slit ($0 < x < h$), as predicted by the GSDE theory [16,14,13], is (cf. eq. (B2) in ref. [13]):

$$\mathcal{F}_{conf}\left[c_f(x)\right] \simeq \frac{a^2}{4}\int_0^h \frac{(\nabla c_f)^2}{c_f}\mathrm{d}x + \int_0^h \frac{c_f(x)}{N}\ln\left(\frac{c_{ref}}{eN}\right)\mathrm{d}x -$$

$$-\frac{2}{N}c_{ref}\eta_0 + \frac{c_b}{Nh}\sum_q f_D(qR)\left|\eta_q\right|^2 \tag{24}$$

where $\eta(x) = \sqrt{c_f(x)/c_{ref}} - c_f(x)/c_{ref}$, $\eta_q = \int_0^h \eta(x)\cos(qx)\mathrm{d}x$, $q = 2\pi n/h$, $n = 0, \pm 1, \pm 2...$, and

$$f_D(k) = \frac{1-(1+k^2)\exp(-k^2)}{k^2-1+\exp(-k^2)}$$

where $k = qR$. Note that c_{ref} is a free parameter of the theory; it is normally chosen as to (nearly) minimize η_0 (to ensure that $\eta(x) \ll 1$ for $x \sim h/2$). In the regime we consider currently $c_f(x)$ is close to c_b everywhere, hence $c_{ref} = c_b$ is the appropriate choice.

Using eq. (21) we get the thermodynamic potential Ω_{conf}:

$$\Omega_{conf}\left[c_f\right] \simeq \frac{a^2}{4}\int_0^h \frac{\left(\nabla c_f\right)^2}{c_f}\mathrm{d}x + \frac{1}{N}\int_0^h \left(\sqrt{c_f} - \sqrt{c_b}\right)^2\mathrm{d}x + \frac{c_b}{Nh}\sum_q f_D(qR)\left|\eta_q\right|^2 \tag{25}$$

where $\eta(x) = \sqrt{c_f(x)/c_b} - c_f(x)/c_b$. Eqs. (24), (25) are applicable if $|\eta_q| \ll R,\ h$.

Taking into account that $c_f(x) \simeq c_b - c_a(x)$, $c_a \ll c_b$, and c_a is defined in eq. (19), we simplify the FPI interaction energy $\Omega(h) \simeq \Omega_{conf}[c_f] + \mathrm{const}$, as

$$\Omega(h) = \frac{c_b}{4Nh}\sum_q \left[1 + k^2 + f_D(k)\right]\left|\varphi(q)\right|^2 \tag{26}$$

where const is omitted, $k = qR$, and

$$\varphi(q) = \frac{2}{c_b}\int_0^\infty c_a^{(1)}(x)\cos(qx)\mathrm{d}x \tag{27}$$

where $c_a^{(1)}(x) \simeq \varkappa c_b f_0(x/R)$ is the single-wall adsorbed profile involved in eq. (19). The function $f_0(\bar{x})$ is defined in eq. (13). Using this equation we obtain

$$\varphi(q) \simeq 2\varkappa R g_D(qR)$$

where

$$g_D(k) = \frac{2}{k^4}\left(k^2 - 1 + \exp(-k^2)\right)$$

is the Debye function. As a result we get the FPI interaction energy between 2 plates at the distance h, $W(h) \equiv \Omega(h) - \Omega(\infty)$: [8]

$$W(h) = \frac{2\varkappa^2 c_b a^2}{R}\omega(h/R) \tag{28}$$

where

$$\omega(\bar{h}) = \frac{1}{\bar{h}}\sum_k g_D(k) - I,\quad I = \int_{-\infty}^{\infty} g_D(k)\frac{\mathrm{d}k}{2\pi} \approx 0.75 \tag{29}$$

$k = 2\pi n/\bar{h}$, $n = 0, \pm 1, ...$ The function $\omega(\bar{h})$ is displayed in Fig. 3 (black solid curve), it monotonically decreases with $\bar{h}$, $\omega(\bar{h}) \simeq 1/\bar{h} - I$ for $\bar{h} \ll 1$, and it vanishes exponentially (as $\bar{h}^{-4}\exp\left(-\bar{h}^2/4\right)$) for $\bar{h} \gtrsim 3$.

The FPI interaction is therefore always repulsive (serving for stabilization) which gets stronger at shorter $h \ll R$. Physically, this is a *depletion* repulsion: it is related to a progressive depletion

[8] The interaction potential is shifted in order to have $W(\infty) = 0$.

of the free chain concentration c_f in the slit as h decreases. In fact, $c_f/c_b \simeq 1 - 2\varkappa R/h$ for $h \ll R$ (at, say, $x = h/2$), while the total concentration c remains constant there ($c \simeq c_b$).

The theory developed above is applicable as long as $\eta(h/2) \ll 1$, that is for $c_a/c_b \ll 1$ corresponding to $h/R = \bar{h} \gg 2\varkappa$. The following generalization can be applied to treat the regime $\bar{h} \sim \varkappa \ll 1$: It is enough to simply change c_{ref} in eq. (24) to $c_{ref} \simeq \beta c_b$ with $\beta \equiv 1 - h^*/h$, which is close to the mean c_f in the slit (as long as $h \gg \xi$). Here

$$h^* \equiv 2\Gamma_a/c_b \simeq 2\varkappa R \tag{30}$$

For $h \ll R$ the first and the last terms in eq. (24) become negligible, so for $h^* < h \ll R$ the remaining terms lead to

$$W(h) + \frac{2I\varkappa^2 c_b a^2}{R} \simeq \Omega_{conf} \simeq \mathcal{F}_{conf} + \frac{hc_b}{N}\left(-\beta \ln \frac{c_b}{N} + 1\right) \simeq$$

$$\simeq \frac{hc_b}{N}\left(1 - \beta + \beta \ln \beta\right), \quad \beta = 1 - h^*/h \tag{31}$$

Note that the above equation is valid also for h comparable with h^*, and that eq. (31) agrees with eq. (28) for $h \gg h^*$. The general result including all terms in eq. (24) is obtained based on eqs. (28), (31):

$$W(h) \simeq \frac{2\varkappa^2 c_b a^2}{R}\omega_\varkappa(h/R), \quad h > h^* \tag{32}$$

where

$$\omega_\varkappa(\bar{h}) = \omega(\bar{h}) - \frac{1}{\bar{h}} + \frac{1}{\varkappa}\left[1 + \left(\frac{\bar{h}}{2\varkappa} - 1\right)\ln\left(1 - \frac{2\varkappa}{\bar{h}}\right)\right] \tag{33}$$

Note that $\omega_\varkappa(\bar{h}^*) \simeq \frac{1}{\varkappa} - I$ for $\varkappa \ll 1$. The function $\omega_{0.2}(\bar{h})$ is also shown in Fig. 3 (red curve). It is clear that the repulsion becomes stronger for $\varkappa > 0$: the potential energy increases more than twice at $h \approx h^*$ as compared with the universal prediction for $\varkappa = 0$.

Eq. (32) is not applicable for $h < h^*$ since the incompressibility condition (20) is violated in this regime: Here the mean concentration of adsorbed chains exceeds c_b, so adsorbed layers are compressed while the free chains are almost totally expelled from the slit. This is the regime of a steric stabilization where the thermodynamic potential is dominated by the excluded-volume part, eq. (22)

$$\Omega_{int}(h) \simeq h\widetilde{f}_{int}(c_b h^*/h)$$

where $\widetilde{f}_{int}(c) = f_{int}(c) - \mu_{int}(c_b)c + \Pi_{int}(c_b)$, and the total interaction energy

$$W(h) = \Omega_{int}(h) + \Omega_{conf}(h) - \Omega_{conf}(\infty) \simeq$$

$$\simeq \left(\frac{v}{2} + \frac{w}{6}c_b(h^*/h + 2)\right) c_b^2 \left(h^*/h - 1\right)^2 h + \frac{c_b}{N}\left(h - I\varkappa h^*\right) \tag{34}$$

increases strongly for $h < h^*$. Noteworthy, the subdominant second conformational term remains positive (therefore, works for stabilization) for $h > 0.75\varkappa h^* \simeq 1.5\varkappa^2 R$, i.e. also for separations well below h^*. For $h^*/h - 1 \ll 1$ eq. (34) gives

$$W(h) \simeq \frac{2\varkappa^2 c_b a^2}{R}\left[\frac{X}{2\varkappa}\left(\frac{h^*}{h} - 1\right)^2 + \omega_\varkappa(\bar{h}^*)\right] \tag{35}$$

where $X \equiv v^* c_b N$ is the reduced interaction parameter and

$$v^* = v + wc_b \tag{36}$$

The reduced potential $W(h)$ for $h < h^*$ is also shown in Fig. 3 with dashed lines (for $X = 10$ and 20).

Thus, the interaction between solid surfaces considered in this section can be described as the free polymer induced depletion repulsion (enhanced due to the soft layer of adsorbed chains) for $h > h^*$ and as the steric repulsion for $h < h^*$.

4. The effect of different lengths of adsorbed and free chains on the FPI interactions

Let us generalize the theory to the case when the molecular weights of adsorbed and free chains are different. This situation can be achieved, for example, by incubating the colloidal particles in a polymer solution with polymerization index N_a to form the adsorbed layers, and then by replacing the free polymer with chains of a different polymerization index $N_f = N$. In this case the adsorbed layer thickness is defined by the size $R_a = a\sqrt{N_a} = n_a R$, where $R = a\sqrt{N}$ is the coil size (gyration radius) of free chains, $n_a = R_a/R = \sqrt{N_a/N}$. The layer density is then controlled by the parameter

$$\varkappa = \frac{\sigma_a}{a^2 c_b} R_a$$

so the adsorbed layer profile for $\varkappa \ll 1$ is (cf. eq. (13)):

$$c_a^{(1)}(x) = \varkappa c_b f_0(x/R_a)$$

and

$$\varphi(q) = \frac{2}{c_b}\int_0^\infty c_a^{(1)}(x)\cos(qx)\mathrm{d}x = 2\varkappa R_a g_D(qR_a)$$

The FPI interaction potential is defined in eq. (26) leading to:

$$W(h) \equiv \Omega(h) - \Omega(\infty) = \frac{2\varkappa^2 c_b a^2}{R}\omega(h/R, n_a)$$

$$\omega(\bar{h}, n_a) = \frac{n_a^2}{\bar{h}}\sum_k \frac{g_D(kn_a)^2}{g_D(k)} - I(n_a), \quad I(n_a) = n_a^2\int_{-\infty}^{\infty}\frac{g_D(kn_a)^2}{g_D(k)}\frac{\mathrm{d}k}{2\pi} \tag{37}$$

Note that the reduced potential $\omega(\bar{h}, n_a) = \omega(\bar{h})$ for $n_a = 1$. It is of interest to reveal the asymptotic behavior of the reduced potential for $n_a \gg 1$ and $n_a \ll 1$. For $n_a \gg 1$ the interaction energy is always positive and decays monotonically with h:

$$\omega(\bar{h}, n_a) \sim \begin{cases} n_a^2/\bar{h} & , \ \bar{h} \ll n_a \\ n_a\,(n_a/\bar{h})^8 \exp\left(-(\bar{h}/n_a)^2/8\right) & , \ \bar{h} \gg n_a \end{cases} \quad (n_a \gg 1) \tag{38}$$

For $n_a \ll 1$ the behavior is more interesting: In this case the adsorbed layers are thin, so for $\bar{h} \gg n_a$ the interaction is similar to depletion repulsion between non-adsorbing surfaces in a semidilute solution [16,14]:

$$\omega(\bar{h}, n_a) \simeq (n_a^2/2)\, u_{int}(\bar{h}), \quad \bar{h} \gg n_a, \quad n_a \ll 1 \tag{39}$$

where the function u_{int} is defined in ref. [16]. However, a strong potential well ($\omega < 0$) is found for $\bar{h} \lesssim n_a$. This attractive well is a purely ground-state dominance (GSD) effect generated by the square-gradient term (the first term in the r.h.s. of eq. (24)). The concentration gradients coming from the two opposite adsorbed layers nearly compensate each other at $x \sim h/2$ leading to a negative contribution to the GSD free energy, and the magnitude of this contribution increases with the degree of overlap between the layers which strengthens at shorter h. With this GSD effect eq. (39) should be amended:

$$\omega(\bar{h}, n_a) \simeq (n_a^2/2)\left[u_{int}(\bar{h}) - (\mathrm{const}/n_a^3)\,(n_a/\bar{h})^6 \exp\left(-(\bar{h}/n_a)^2/8\right)\right], \quad \bar{h} \gg n_a, \quad n_a \ll 1$$

The attraction dominates for $n_a^2 \lesssim \bar{h} \lesssim 4n_a\sqrt{\ln(1/n_a)}$. [9]

---

[9] Note that the above equation is useful to highlight the asymptotic behavior of the function $\omega(\bar{h}, n_a)$. However, for its numerical calculations the exact eq. (37) should be used instead.

In practice, the most relevant case is $n_a \sim 1$. The reduced potential was calculated numerically for several $n_a \sim 1$. The results are shown in Fig. 4. The depletion repulsion is obviously enhanced for $n_a > 1$. For $n_a < 1$ an attraction region (energy well) is developed. However, the attraction is negligible for $n_a > 0.8$ (the depth of the well is smaller than 1/200). For $n_a < 0.8$ the well depth rapidly grows, while its position shifts to smaller $\bar{h}$.

We stress that the FPI interaction considered here is always of depletion nature (related to the entropy of free chains), including the depletion repulsion predicted for $n_a \gtrsim 0.8$ and depletion attraction for $n_a \lesssim 0.8$.

5. FPI interaction for high concentration of attractive centres

The case of high concentration of adsorbing centres, $\varkappa \gg 1$, is considered using the SCFT approach [13] for different N_a/N. A slight generalization of the model is applied here: we allow for an increase of the polymer bulk concentration (from c_{b0} to c_b) after formation of the adsorbed polymer layer. It is assumed (now as an approximation) that the adsorbed polymer profile is still given by the reflection procedure, eq. (19), with

$$c_a^{(1)}(x) = c_{b0} f_1(x/R_a)$$

(cf. eq. (15)), and that, accordingly, the boundary conditions for free chains at the solid surfaces are of the Neumann type, eqs. (2), (5). The reduced adsorbed profiles, $c_a(x)/c_{b0}$ vs. x/R_a, are shown in Fig. 5 for different $h/R_a = 0.6,\ 1.4,\ 2.8,\ 3.8,\ 10$. It is clear that for large $h \gtrsim 5R_a$ the adsorbed polymer is localized near the surfaces, while its concentration becomes nearly uniform for $h \lesssim R_a$. Note that the area under the curves is always the same $(= 2/\sqrt{\pi})$.

The FPI interaction potential generally scales as (cf. eq. (28))

$$W(h) = \frac{c_b a^2}{R} \bar{W}(h/R) \tag{40}$$

As argued in section 3 the polymer solution can be viewed as nearly incompressible (see eq. (20)) in a semidilute or concentrated regime (i.e., for $X \equiv v^* c_b N \gg 1$) at the length-scales beyond the correlation length, $h \gg \xi$. Therefore, the FPI potential is not expected to depend strongly on the virial parameters in this regime. This point is validated by our SCFT results for the reduced potential shown in Fig. 6 for different X and $r_b = c_{b0}/c_b$. The dependence of W on X was therefore disregarded in further calculations.

The reduced FPI potentials for different $r_b = c_{b0}/c_b$ and $n_a = 1$ (adsorbed and free chains are the same) are shown in Fig. 7. It is obvious that the FPI interaction is always repulsive here. As one would expect, $W(h)$ gets stronger and its range increases at larger r_b. The potential curves are similar, but seem to be shifted with respect to each other along both axes. The curves can be superimposed rather well by rescaling both W and h (not shown).

For $r_b \ll 1$ the SCFT results can be verified analytically. In this case $c_a \ll c_b$, so the concentration profile of free chains, $c_f(x)$, is only weakly inhomogeneous. Therefore, eq. (26) becomes applicable together with eq. (27) (by virtue of the incompressibility condition (20)). Thence we get

$$\bar{W}(h) \simeq \frac{1}{4} r_b^2 n_a^2 w_{int}(h/R) \tag{41}$$

where

$$w_{int}(\bar{h}) = \frac{1}{\bar{h}} \sum_k \left[1 + k^2 + f_D(k)\right] |\varphi_1(k n_a)|^2$$

$$\varphi_1(z) = 2 \int_0^\infty f_1(x) \cos(zx) \mathrm{d}x$$

and $k = 2\pi n/\bar{h}$, $n = 0, \pm 1, \ldots$ as before. Using eq. (15) we find

$$\varphi_1(z) = \frac{8}{\sqrt{\pi}} z^{-3} \left[2D_+(\frac{z}{2}) - D_+(z)\right]$$

where

$$D_+(z) = e^{-z^2} \int_0^z e^{z^2} \mathrm{d}z$$

is the Dawson function. [10] Eq. (41) predicts that the reduced potential $\bar{W}$ should scale as r_b^2 for $r_b \ll 1$. The SCFT results are compared in Fig. 8 with the analytical prediction, eq. (41), for $n_a = 1$. A good agreement can be observed for $r_b \lesssim 0.1$, while more generally the asymptotic analytical curve slightly underestimates the repulsion magnitude (for $r_b \lesssim 0.2$).

The dependence of the interaction potential on the adsorbed layer thickness (n_a) is shown in Fig. 9. The qualitative picture is similar to what was predicted in the previous section for more dilute adsorbed layer, $\varkappa \ll 1$: The interaction is always repulsive for $n_a \gtrsim 0.8$, while for $n_a \lesssim 0.8$ a local potential well is developed. Its depth increases sharply as n_a is further decreased (see Fig. 10a). Simultaneously, the range of attraction shifts to shorter h (see Fig. 11).

The repulsion regime is formally re-entered at even shorter distances. However, this short-range repulsion is not useful for stabilization (in view of the deep potential well at larger h) and it is not resolved numerically for $n_a \lesssim 0.1$. The attraction region (for $n_a \lesssim 0.8$) is preceded by the distal repulsion barrier (at longer separations h) whose height is not large (see Fig. 10b). Both the repulsion and attraction interaction forces demonstrated here originate from the FPI effect due to the confinement dependence of the conformational free energy of free chains.

The leftmost solid curve in Fig. 9 corresponds to the potential $W_{pr}(h)$ for purely repulsive solid surfaces [13] with no soft adsorbed layer at all. It is interesting that the potential curves for low n_a tend to $W_{pr}(h)$. This may seem a bit surprising as the Neumann boundary conditions (eq. (5)) are applied in the case of the soft layer, while the conditions are of Dirichlet type ($\psi(0) = 0$) for the purely repulsive surfaces. The explanation is rather simple: in the limit $n_a \ll 1$ the adsorbed layer is thin hence the adsorbed chains do not affect the free chains outside this thin layer. On the other hand, the presence of a however thin adsorbed layer (of course, it is always assumed that its thickness exceeds the monomer size) prohibits a considerable penetration of free monomers down to the solid surface and leads to the *effective* boundary condition $\psi = 0$ for free chains at the surface. This is why $\bar{W}(\bar{h}) \to \bar{W}_{pr}(\bar{h})$ for $n_a \to 0$ (and $X \to \infty$).

6. Interaction between spherical particles

6.1. Distal region

We are now in a position to evaluate the FPI interaction between spherical particles of diameter D_c assuming $D_c \gg R$. By virtue of the Derjaguin approximation the interaction energy is

$$U(h) \simeq (\pi/2) D_c \int_h^\infty W(h) \mathrm{d}h \tag{42}$$

The FPI solvation force is

$$F(h) = -\frac{\partial U}{\partial h} = (\pi/2) D_c W(h)$$

Let us consider as before the regime of relatively large separations, $h \gtrsim R \gg \xi$. Based on the results of the previous sections, we therefore predict that in this regime the FPI solvation force is essentially always repulsive $F(h) \geq 0$ if $n_a = R_a/R > 0.8$, i.e., if the adsorbed layer thickness is not too small compared to the free coil size R.

Eq. (42) can be rewritten using eq. (40) as

$$U(h) \simeq A_R \bar{U}(\bar{h}),$$

where

$$A_R = (\pi/2) D_c c_b a^2 = \frac{\pi}{12} D_c \phi_b a_s^2 / v_1 \tag{43}$$

---

[10] Thus, the function $\varphi_1(z)$ is an analytical function of z, $\varphi_1(0) = 4/\sqrt{\pi}$, $\varphi_1(z) \simeq 12 z^{-4}/\sqrt{\pi}$ for $z \gg 1$.

is the characteristic interaction energy (in k_BT units), and

$$\bar{U}(\bar{h}) = \int_{\bar{h}}^{\infty} \bar{W}(\bar{h})\mathrm{d}\bar{h}$$

For example, with $D_c = 200$nm the constant A_R according to eq. (43) is $A_R \approx 80$ for polystyrene (PS) solution in toluene, $\phi_b = 0.5$ ($a_s \approx 7.5\mathring{A}$, $v_1 \approx 180\mathring{A}^3$ [13]) or for PEO in water, $\phi_b = 0.3$ ($a_s \approx 5.5\mathring{A}$, $v_1 \approx 65\mathring{A}^3$ [13]). Assuming that the monomer volume $v_1 \sim a_s^3$, we can estimate it as $A_R \sim \phi_b D_c/a_s$.

The FPI potential is plotted in Fig. 12(a) for $A_R = 80$, $\varkappa \gg 1$, $r_b = 1$ and different n_a. It is clear that the energy well which is developed at $h \gtrsim 2R$ is unimportant if $n_a \gtrsim 0.6$ (in this case the well depth is less than $\sim 1.5k_BT$, so colloid destabilization is avoided [1]) [11]. More precisely, the stability criterion is $n_a > n^*(A_R)$, where the critical $n^* < 1$ is slightly increasing with A_R: for example, $n^* \approx 0.6$ for $A_R \sim 80$, and $n^* \approx 0.7$ for $A_R \sim 400$.

For the opposite regime of low density of attractive centres, $\varkappa \ll 1$, we obtain using eqs. (42), (37):

$$U(h) \simeq 2\varkappa^2 A_R \int_{\bar{h}}^{\infty} \omega(\bar{h}, n_a)\mathrm{d}\bar{h} \tag{44}$$

The corresponding potential curves are plotted in Fig. 12(b) for $\varkappa^2 A_R = 10$ and different n_a. In this case the critical n_a is $n^* \approx 0.6$, while it increases to $n^* \approx 0.7$ for $\varkappa^2 A_R = 30$.

Let us now consider the total interaction potential $U_{tot}(h) = U(h) + U_H(h)$ including both the FPI potential and the van der Waals attraction [36]

$$U_H(h) = -\frac{A_H D_c}{24h} \tag{45}$$

where A_H is the Hamaker constant. The total potential is shown in Fig. 13 using the FPI interaction data from Fig. 12(a) for $D_c = 200$nm, $R \approx 3$nm (corresponding to PS chains with polymerization index $N \approx 100$) and $A_H = 1\ k_BT$ (roughly corresponding to PS latex in toluene [35]). [12] One can observe that in this case the FPI depletion repulsion imparts colloid stabilization for $n_a \gtrsim 0.7$.

6.2. The proximal region: depletion repulsion vs. depletion attraction

So far we considered the interaction at distances exceeding the solution correlation length, $h \gg \xi$, neglecting the short-range contribution to $W(h)$ effective at $h \sim \xi$. In the general case the GSDE theory predicts [13,14]

$$W(h) \simeq W_e(h) + W_{gs}(h) \tag{46}$$

where $W_e(h)$ is the long-range contribution calculated above (see eqs. (28), (40), and $W_{gs}(h)$ is the classical short-range interaction obtained within the GSD approximation. For purely repulsive walls the GSD result (established in ref. [13] using the third virial approximation, eq. (23)) is

$$W_{gs} \simeq -A^2 c_b a^2 \xi^{-1} e^{-h/\xi} \tag{47}$$

where $A = 4(1 + 1/\alpha)$, $\alpha = 2 + 3v/(c_b w)$, and ξ is defined in eq. (1). Note that for $h \sim \xi$ we need not distinguish between free and adsorbed chains since both the free chain size and the size of the typical (dominating by mass) loops/tails of adsorbed chains are much larger than h. Eq. (47) represents the asymptotic behavior of W_{gs} for $h \gg \xi$. It is sufficient for our analysis since normally h/ξ is large in the region of interest where the two terms in eq. (46) compete. [13]

There is another physical restriction on eq. (47): it is valid as long as there is equilibrium between the slit and the bulk solution that is if some free chains do penetrate into the slit. This

---

[11] At this stage we neglect the van der Waals (vdW) attraction between colloidal particles assuming that they are matched dielectrically with the solvent.

[12] Note that A_H for the hydrocarbon/water media pair is not much larger, $A_H \sim 1 - 2k_BT$, [36].

[13] The reason is that W_{gs} always dominates over W_e at $h \sim \xi$ in the regime of interest, $\varkappa \lesssim 0.5$.

is not the case any more (within the GSD approximation) for $h < h^*$, where $h^* = 2\Gamma_a/c_b$ and $2\Gamma_a$ is the total amount of adsorbed polymer in the slit. At such high compression we return to the classical steric repulsion: $W(h)$ is approximately given by the excess energy of monomer interactions in the slit

$$W(h) \simeq \left(\frac{v}{2} + \frac{w}{6} c_b (h^*/h + 2)\right) c_b^2 \left(h^*/h - 1\right)^2 h, \quad h < h^* \tag{48}$$

For $n_a = 1$ and small $\varkappa$ the FPI interaction energy between two spherical particles (D_c) reads (cf. eq. (46)):

$$U_{FPI}(h) = U_e(h) + U_{gs}(h), \quad h > h^* \tag{49}$$

where

$$U_e(h) \simeq 2\varkappa^2 A_R \int_{\bar{h}}^{\infty} \omega_\varkappa(\bar{h}) \mathrm{d}\bar{h}$$

$\omega_\varkappa(\bar{h})$ is defined in eq. (33), $h^* = 2\varkappa R$ and

$$U_{gs}(h) \simeq -A_R A^2 e^{-h/\xi} \tag{50}$$

The reduced FPI potential, U_{FPI}/A_R, calculated using eqs. (49), (33), (50) for different ξ/R and $\varkappa$, is plotted against h/h^* in Fig. 14. It is clear that the effect of depletion repulsion prevails (against attraction) for larger $\varkappa$ or for shorter ξ.

For $\varkappa \ll 1$ the interaction potential $U_{FPI}(h)$ can be also obtained analytically in the region $h \ll R$ (since the critical region of the emerging potential well corresponds to $h/R \approx h^* \simeq 2\varkappa$). In this case eq. (33) can be simplified as

$$\omega_\varkappa(\bar{h}) = \frac{1}{\varkappa}\left[1 + \left(\frac{h}{h^*} - 1\right) \ln\left(1 - \frac{h^*}{h}\right)\right]$$

On using also eqs. (49), (50) we obtain

$$U_{FPI}(h) \simeq A_R \left\{2\varkappa^2 \ln\frac{R}{h} - A^2 e^{-h/\xi}\right\} \tag{51}$$

This dependence can be illustrated by the curves in Fig. 14(a). Note that eq. (51), valid for $h \ll R$, is in agreement with the results of the previous section, eq. (44) for $n_a = 1$, valid for $h \gg \xi$ (i.e., the two analytical predictions cross over smoothly and agree in the region $\xi \ll h \ll R$ where their validity regions overlap).

The following conclusions can be drawn based on this result: In the absence of a vdW attraction the thermodynamic stabilization of the system (i.e., suppression of the depletion flocculation) is expected if a potential well does not develop at $h \approx h^*$, i.e. if $A^2 e^{-h^*/\xi} < 2\varkappa^2 \ln(R/h^*)$, roughly leading to the following criterion

$$\xi/R < \varkappa/\ln(3/\varkappa), \quad \varkappa \ll 1 \tag{52}$$

If the above condition is violated, a stabilization of kinetic nature is still possible provided that the energy barrier U^* is high enough, $U^* \gtrsim 15$. From eq. (51) we deduce $U^* \simeq 2A_R\varkappa^2 |\ln(2\varkappa)|$. Then, for example, for $\varkappa = 0.3$ the FPI stabilization may be expected either if $\xi/R < 0.15$, or if $A_R \gtrsim 80$ (the latter condition follows from the requirement $U^* \gtrsim 15$).

Note that the FPI interaction only was considered above. Generally, the full interaction potential is the sum of the FPI and vdW contributions. The vdW attraction can be added to the FPI potential to obtain the total interparticle potential for a particular colloidal system once the relevant Hamaker constant is known.

7. Discussion and Conclusions

1. In this paper we considered the free polymer induced (FPI) interactions between colloidal particles dispersed in a polymer solution. The surfaces of the particles are decorated with some strongly attractive sites able to trap polymer segments. The self-assembled adsorbed polymer

layers are thus formed around the particles. It is shown that interaction of free polymer with these fluffy layers gives rise to a depletion repulsion force between colloidal particles. This depletion interaction is due to a redistribution of free polymer chains (their depletion inside the soft layers) implying progressively higher entropic cost at shorter separations h between colloidal particles. The repulsion therefore stems from the excess ideal-gas free energy of unattached chains. The effect is significant in the semidilute or concentrated solution regime where polymer coils overlap strongly, $c_b \gg c_{ov}$, so that the polymer correlation length ξ is small compared to the coil size R, $\xi \ll R$ (in the marginal solvent regime this condition reduces to $X \equiv v^* c_b N \gg 1$, where v^* is the effective monomer interaction parameter, cf. eq. (1)). [14]

2. The structure of the fluffy layer is analyzed both in the case of instant anchoring of polymer segments near the traps and as a result of the adsorption process with reaction-controlled kinetics (the latter is relevant if the polymer/surface bond formation is a slow activation process). We establish that the resultant adsorbed concentration profile $c_a(x)$ is the same in both cases, being related to the equilibrium polymer distribution in the presence of an auxiliary potential field localized near the solid surfaces. Moreover, it turns out that the profile $c_a(x)$ is rather universal (as long as the considered length-scale exceeds ξ): the profile depends essentially on the single parameter $\varkappa$ which is proportional to the surface concentration σ_a of adsorbing sites and to $R \propto \sqrt{N}$ (cf. eqs. (11), (13), (15)). The total adsorbance Γ_a increases with $\varkappa$ for $\varkappa \lesssim 1$ (see eq. (14)) and saturates for $\varkappa \gg 1$ (Γ_a is the total number of repeat units belonging to adsorbed chains per unit area). Interestingly, the crossover regime $\varkappa \sim 1$ corresponds to a low surface concentration of attractive sites in the case of long chains, $N \gg 1$.

The effective thickness $h^*/2$ of the fluffy layer is proportional to the surface coverage: $h^*/2 = \Gamma_a/c_b$; h^* always increases with the chain length N (cf. eqs. (14), (16)):

$$h^* \simeq \begin{cases} 2N\sigma_a/c_b & , \ \varkappa \ll 1 \\ (4/\sqrt{\pi})a\sqrt{N} & , \ \varkappa \gg 1 \end{cases} \tag{53}$$

3. At $h > h^*$ the free polymer necessarily penetrates in the gap region in order to maintain the total concentration $c(x)$ there nearly equal to c_b ($c(x) = c_a(x) + c_f(x)$; note that $c(x)$ must be exactly uniform in the limit $v^* c_b N \to \infty$). Therefore, the free energy of excluded-volume interactions is constant (independent of h) in this regime. The conformational free energy of adsorbed chains is also nearly constant. [15] The polymer-induced repulsion in this regime is therefore primary due to the excess conformational free energy of unattached (free) polymer chains.

Noteworthy, the condition $c(x) = c_b$ eliminates the concentration contrast between the soft layers and the bulk solution, hence the presence of soft layers does not lead to an increase of the effective range of the vdW attraction (unlike the case of the classical steric stabilization where the attraction range can be enhanced by the thickness of attached polymer layers).

4. It is important to distinguish the FPI depletion repulsion, which is operative at $h > h^*$, from the polymer-induced steric repulsion. The steric repulsion is not effective at $h > h^*$, but is at work for shorter h. For $h < h^*$ the mean concentration of adsorbed polymer in the gap h between the solid surfaces exceeds the bulk concentration c_b, hence the repulsive solvation force is due to a significant increase of the free energy of excluded-volume interactions between polymer units inside the gap. In this regime the free polymer does not penetrate in the gap any more (apart from an exponentially small amount for $v^* c_b N \gg 1$). Physically, the stabilization effect for $h < h^*$ is thus due to the repulsion between compressed adsorbed layers. In particular, for $1 - h/h^* \ll 1$ the repulsive solvation force is proportional to (cf. eq. (48)) $W(h) \simeq 0.5 v^* c_b^2 h^* (1 - h/h^*)^2$.

5. The main results on the polymer effect for colloidal interactions can be summarized as follows. Three FPI mechanisms are generally predicted here: long-range depletion repulsion (for $h > h^*$), steric repulsion (for $h < h^*$) and short-range depletion attraction (for $h \lesssim \xi$). The first two mechanism are associated with the soft surface layers.

The soft layer is unimportant (too thin or dilute) if $h^* \ll \xi$, so the results for naked colloidal particles [13] are applicable in this case of relatively minor interest: Here the FPI interaction is repulsive for $h \gtrsim 10\xi$, while depletion attraction is effective at smaller separations. The energy

---

[14] Note that the theory which formally requires the marginal solvent regime for the free polymer, is applicable not only for marginal solvents near the theta-point, but also for practically good solvents (like toluene for polystyrene) as discussed at the beginning of section 2.1.

[15] This statement can be rigorously proved for $\varkappa \ll 1$.

barrier due to the long-range depletion repulsion is normally not sufficient to render kinetic stabilization of colloidal systems against vdW and depletion flocculation effects. [13]

However, the situation is different if $h^* \gtrsim \xi$. Three interaction regimes can be distinguished in this case: (i) depletion repulsion dominates at $h \gg h^*$, (ii) two opposite depletion effects can compete at $h \gtrsim h^*$, (iii) steric repulsion dominates over depletion attraction for $h < h^*$. The colloidal stability is defined mostly by the competition regime (ii). Then, the general condition of thermodynamic stability can be obtained based on the FPI interaction potential calculated in sections 6.1, 6.2 for $\varkappa \gg 1$ and $\varkappa \ll 1$ (cf. eq. (52)):

$$\xi/R \lesssim \min\left(\varkappa/\ln(3/\varkappa), 0.5\right) \tag{54}$$

This condition is roughly equivalent to $\xi \lesssim h^*$ (cf. eq. (53)). The criterion (54) shows that the thermodynamic stability increases as ξ/R gets smaller, or as $\varkappa$ gets larger. Both tendencies are illustrated in Fig. 14: Fig. 14(a) shows that stabilization is expected for $\varkappa > 0.3$ if $\xi/R = 0.125$, while Fig. 14(b) indicates that for $\varkappa = 0.5$ the stability is achieved for $\xi/R < 0.25$.

Recalling that ξ/R decreases and $\varkappa$ increases with N we conclude that the FPI thermodynamic stabilization (in the presence of fluffy adsorbed layers) can be always achieved with sufficiently long polymer chains. This is in contrast to the case of colloidal particles with naked surfaces [13] where an indefinite increase of N rather leads to an opposite effect: a suppression of the FPI repulsion (and the corresponding energy barrier) and eventual destabilization of the colloidal system.

6. It is noteworthy that the criterion (54) can be rewritten as $N > N^*$. The critical chain length N^* depends on concentration c_b and other parameters. Omitting numerical and log factors for simplicity, we get using eqs. (54), (1), (11):

$$N^* \sim \begin{cases} a\sqrt{c_b}/\left(\sigma_a\sqrt{v^*}\right) & , \ c_b \gtrsim c_1 \sim \sigma_a^{2/3}/\left(v^* a^2\right)^{1/3} \\ 1/\left(c_b v^*\right) & , \qquad c_b \lesssim c_1 \end{cases} \tag{55}$$

The corresponding region of colloidal stability is shown schematically in Fig. 15 with variables c_b, N. It shows that the depletion repulsion is not strong enough for short chains, $N < N_1$, where the threshold $N_1 \sim \left(\frac{a}{\sigma_a v^*}\right)^{2/3}$ increases at low σ_a. Remarkably, the diagram also shows that there is an optimal stabilization concentration c_1 which is proportional to $\sigma_a^{2/3}$, so c_1 can be low for small surface concentration of adsorbing sites. At $c = c_1$ the depletion stabilization is effective for the widest range of molecular weights, $N > N_1$. Note that for $c_b \ll c_{max}$ the phase diagram is nearly universal in the reduced variables N/N_1 vs. c_b/c_1.

Turning to the concentration dependence of the FPI effect, the diagram of Fig. 15 predicts a finite concentration window of stability at $c^* < c_b < c^{**}$, where $c^* \sim c_1 N_1/N$, $c^{**} \sim c_1 \left(N/N_1\right)^2$. The system is unstable outside this window, for $c < c^*$ and for $c > c^{**}$ (of course, c^{**} could formally grow beyond the maximum concentration $c_{max} = 1/v_1$; in this case the second instability region disappears). A similar sequence of effects (stabilization, destabilization) due to an increase of the added polymer concentration have been observed in certain colloidal systems [1]. It is reminiscent of the re-entrant solidification by varying temperature observed in classical polymer-colloid depletion systems and predicted with classical depletion and bridging interactions [7]. Our results (cf. Fig. 15) show that polymer concentration can be used instead of temperature to produce a similar effect.

7. It is remarkable that the FPI depletion repulsion predicted in this study is strongly enhanced due to the presence of adsorbed fluffy layers. This is true for $c_b \gg c^*$, i.e. when $R \gg \xi$. Indeed, let us compare the magnitudes of the depletion repulsion energy in the cases when the colloidal surface is naked and impenetrable and when it is covered by a soft adsorbed layer. In the naked case the energy is proportional to [13,14] $U_{naked}/D_c \sim c_b \xi^2/N$, while in the soft layer case $U_{soft} \sim \varkappa^2 c_b a^2$ for $\varkappa \lesssim 1$ (cf. eqs. (43), (44)). Therefore

$$U_{soft}/U_{naked} \sim \varkappa^2 R^2/\xi^2, \quad \varkappa \lesssim 1 \tag{56}$$

and, in particular, $U_{soft}/U_{naked} \sim v^* N c_b \gg 1$ for $\varkappa \sim 1$. The enhancement ratio increases further (for numerical reasons) and saturates in the case of denser layers, $\varkappa \gtrsim 1$. Therefore, the presence of soft layer significantly strengthens the FPI repulsion if $\xi/R \ll \min(\varkappa, 1)$. The latter condition is roughly equivalent to $N \gg N^*$, so it can be always satisfied with long enough chains, even if the surface concentration σ_a of attractive sites is low. It is therefore revealed that the steric and depletion stabilization mechanisms work cumulatively in the case of partial polymer adsorption, giving rise to a significant enhancement of the overall stabilization effect.

8. Let us consider the solvent quality effects. The results of this paper show that the FPI stabilization assisted by soft surface layers is more efficient in better solvent conditions: the threshold N^* (defining the onset of stabilization, cf. eqs. (55)) always decreases as the solvent quality defined by v^* is increased. In other words, the regime of basically repulsive FPI interaction potential (with no or negligible attraction wells) is established for higher solvent quality (as N^* decreases below the chain length N following an increase of v^*).

Turning to temperature dependence of the depletion stabilization effect, that N^* depends on T mainly via the effective virial parameter v^* (N^* decreases with v^*, cf. eq. (55)). In the athermal good solvent regime v^* is nearly independent of T, and so is N^*. However, in the marginal solvent regime (this paper is focussed on) v^* normally depend on T due to a competition between steric repulsion and enthalpic attraction of polymer segments. A temperature increase normally leads to a better polymer solubility (higher v^*), hence giving rise to an improved colloidal stability (lower N^*).

9. The theoretical results summarized above can provide a tentative explanation of certain striking observations concerning the effect of poly(ethylene oxide) (PEO) aqueous solutions on interactions between solid surfaces. There are contradictory evidences on whether the added PEO adsorbs on the glass or polystyrene surfaces, and whether it imparts a depletion attraction or not. [37,38] The model involving surface traps (σ_a) considered in the present paper allows for both behaviors, the control parameter being N/N^*. The adsorbed layer is negligible (too dilute) if N/N^* is small, hence the classical depletion attraction is dominated in this case. By contrast, for large N/N^* the adsorbed layer is considerable, and *depletion repulsion* wins. For $c > c_1$ the ratio N/N^* is proportional to $N\sigma_a$ (cf. eq. (55)). Therefore, for the given surfaces, an attraction is expected for short PEO chain and repulsion for long chains. Moreover, for a fixed N both behaviors are also possible if σ_a is varied.

Our results are also consistent with the findings [19,20] that small concentrations of high molecular weight free PEO can provide (or significantly contribute to) the stabilization of gold nanoparticles in aqueous solutions. To apply the model we hypothesize that some PEO segments can adsorb onto gold surface. [21] [16] For $c < c_1$ the predicted stability criterion ($N/N^* > 1$) leads to the condition $Nc >$ const in agreement with experimental results [19] on stability of AuNPs for different PEO concentrations and molecular weights.

10. The theory of this paper is also generalized to comprise the systems with different length of adsorbed (N_a) and free (N) chains. Such a system can be obtained, for example, if colloidal particles are initially dispersed in solution of N_a-chains, and then free N_a-chains are replaced by the N-chains. It is shown that a significant distal attraction well (as opposed to the proximal minimum at $h \sim \xi$ considered above, see point 5) is developed at $h \sim 2R - 3R$ if adsorbed chains are considerably shorter than free chains. Conversely, the distal attraction is negligible if $\sqrt{N_a/N} > n^*$, where typically $n^* \sim 0.6 - 0.7$ depending on the polymer/colloidal parameters (see Figs. 12, 13). Therefore, the FPI colloidal stabilization in the considered systems is possible if $N_a/N \gtrsim 0.4 - 0.5$.

These predictions are in a qualitative agreement with the results on interaction of micelles in block-copolymer/homopolymer mixtures [40] showing that micelles repel each other if the length N_h of free homopolymers is below a certain threshold, $N_h < N_h^*$, related to the thickness of the copolymer/homopolymer interpenetration layer. Our results also agree qualitatively with the predictions and experimental results [41–43] on interactions between solid surfaces covered with grafted polymer layers (N_g chains) and immersed in a polymer solution (N_f chains): an attraction minimum was predicted there for $N_f > N_f^*$. However, in contrast to our results, the obtained N_f^* was typically shorter than N_g, and it was found to decrease further at higher grafting densities [41]. This discrepancy points to an important difference between the grafted layers considered before and the self-assembled adsorbed layers studied here.

Acknowledgements

A support from the IRTG 'Soft matter science' is gratefully acknowledged.

[16] The reversibility of PEO adsorption onto the gold surfaces seems to be an issue. Here we assume that some PEO fragments can be irreversibly adsorbed on gold nanoparticles due to formation of trains of surface bonds (PEO segments can form H-bonds with citrate molecules covering the gold surface [39,21]).

[1] D.H.Napper, Polymer Stabilization of Colloidal Dispersions Academic, London, 1983.
[2] H.Lekkerkerker, R.Tuiner, Colloids and Depletion Interaction. Springer, 2011.
[3] N. Kozer, Y. Y. Kuttner, G. Haran, G. Schreiber, ***Biophys. J.*** 2007, 92, 2139.
[4] Van Oss C.J., Arnold K., Coakley W.T., ***Cell Biophys.*** 1990, 17, 1.
[5] Alivisatos, A. P.; Gu, W.; Larabell, C. Annu. Rev. Biomed. Eng. 2005, 7, 55-76.
[6] De Gennes P.G., Adv. Colloid. Interface Sci., 1987, v.27, 189;
[7] Feng L., Laderman B., Sacanna S., Chaikin P. Nature Mater. 14, 61 (2014).
[8] De Gennes P.G., Macromolecules 14, 1637 (1981); 15, 492 (1982).
[9] De Gennes P.G., Macromolecules, 1989, v.22, 276.
[10] A.N.Semenov, J.F.Joanny, A.Johner, J.Bonet-Avalos, Macromolecules **30**, 1479 (1997).
[11] Bonet-Avalos J., Joanny J.F., Johner A., Semenov A.N., Europhys. Lett. 1996, 35, 97.
[12] A.Broukhno, B. Jönsson, T.Åkesson, J.Chem.Phys. 113, 5493 (2000).
[13] A.A.Shvets, A.N.Semenov, J.Chem.Phys. 139, 054905 (2013).
[14] Semenov A.N., Macromolecules 41, 2243 (2008).
[15] Vrij A., Pure Appl. Chem. 1976, 48, 471.
[16] Semenov A.N., J.Phys. II Fr. 6, 1759 (1996).
[17] R. Maassen, E. Eisenriegler, and A. Bringer, J. Chem. Phys., Vol. 115, No. 11 (2001)
[18] A. Shvets, Theory of Colloid Stabilization by Unattached Polymers. PhD thesis, Strasbourg, 2014.
[19] X.Zhang, M.R.Servos, J.Liu, JACS 134, 9910 (2012).
[20] N.J.Lang, B.Liu, X.Zhang, J.Liu, Langmuir 29, 6018 (2013).
[21] K.Larson-Smith, D.C.Pozzo, Langmuir 2012, 28, 13157.
[22] S.F.Edwards, Proc.Phys.Soc. 85, 613 (1965).
[23] Lifshitz I.M., Grosberg A.Yu., Khokhlov A.R., Rev. Mod. Phys. 50, 683 (1978).
[24] Grosberg, A.; Khokhlov, A. ***Statistical Physics of Macromolecules***, American Institute of Physics, New York, **1994**.
[25] A.N.Semenov, I.A.Nyrkova. Statistical Description of Chain Molecules. In: Matyjaszewski K and Moeller M (eds.) Polymer Science: A Comprehensive Reference, Vol 1, pp. 3-29. Amsterdam: Elsevier BV (2012).
[26] Polymer Handbook, edited by Brandrup J., Immergut E. H., Grulke E. A., Wiley- Interscience, 1999.
[27] Huber K., Bantle S., Lutz P., Burchard W., Macromolecules 1985, 18, 1461.
[28] P.-G. de Gennes, Scaling Concepts in Polymer Physics, Cornell Univ. Press, Ithaca, 1979.
[29] M. Rubinstein, A.N. Semenov, Macromolecules 1998, 31, 1386.
[30] E.Eisenriegler, K.Kremer, K.Binder, J.Chem.Phys. 77, 6296 (1982).
[31] Eisenriegler, E.; ***Polymers near Interfaces***, World Scientific Publishing, Singapore 1993.
[32] A.E.Likhtman, A.N.Semenov, Europhys. Lett., 2000, v.51, 307.
[33] A.N.Semenov, J.-F.Joanny, A.Johner, In: Theoretical and Mathematical Models in Polymer Science, Chapter 2, pp.37-81 (Ed. A. Grosberg, Academic Press, Boston, 1998).
[34] Edgar M. Blokhuis, Karl Isak Skau, Josep B. Avalos J. Chem. Phys., Vol. 119, 3483 (2003).
[35] Noskov S. et al., J. Chromat. A, 1274, 151 (2013).
[36] J.N. Israelachvili, ***Intermolecular and Surface Forces*** (Academic Press, NY, 1985).
[37] D.Kleshchanok, P.R.Lang, Langmuir 2007, 23, 4332.
[38] D.Kleshchanok, R.Tuinier, P.R.Lang, J.Phys.:Condens.Matt. 2008, 20, 073101.
[39] Wang F.K. et al. Chem. Comm. 2011, 47, 767.
[40] Semenov A.N., ***Macromolecules*** 1993, 26, 2273.
[41] Wijmans C.M., Zhulina E.B., Fleer G.J. Macromolecules 27, 3238 (1994).
[42] Zhulina E.B., Borisov O.V., Brombacher L., Macromolecules 24, 4679 (1991).
[43] Dutta N., Green D. Langmuir 24, 5260 (2008).

FIGURE CAPTIONS

FIG. 1. The dependence of the reduced concentration in the adsorbed layer at the solid surface, $c_a(0)/c_b$, on the reduced surface concentration of attractive sites, $\varkappa$.

FIG. 2. The reduced concentration profiles of adsorbed chains vs. reduced distance, x/R, to a single flat wall: $c_a(x)/(\varkappa c_b) = f_0(x/R)$ for $\varkappa \ll 1$ (curve 1); $c_a(x)/c_b = f_1(x/R)$ for $\varkappa \gg 1$ (curve 2). The second curve actually represents 4 coinciding curves obtained numerically using the SCFT approach for $\delta_b/R = 0.05,\ 0.2,\ 0.5$ as described in the text (the SCFT curves are shifted along the horizontal axis: $c_a(x+\delta_b)/c_b$ is plotted vs. x for each δ_b) and analytically using eq. (15).

FIG. 3. The reduced interaction potential for $\varkappa \ll 1$: $\omega = \frac{R}{2\varkappa^2 c_b a^2} W(h)$ vs. $\bar{h} = h/R$ (cf. eq. (29)). Black curve: ω vs. $\bar{h}$ for $\varkappa \to 0$; red curve: $\omega = \omega_{0.2}(\bar{h})$ for $\varkappa = 0.2$ and $h > h^* = 2\varkappa R$ (cf. eq. (33)). Dashed curves (calculated using eq. (35)): the short distance part ($h < h^*$) of the reduced potential for $\varkappa = 0.2$ and $X \equiv v^* c_b N = 10$ (dashed blue), $X = 20$ (dashed black).

FIG. 4. The reduced interaction potential $\omega = \frac{R}{2\varkappa^2 c_b a^2} W(h)$ vs. $\bar{h} = h/R$ for $\varkappa \ll 1$ and different n_a. The potential was calculated using eq. (37). (a) The curves for $n_a = 0.4$, 0.6, 0.7, 0.8, 1, 1.2, 1.5, 2 (from left to right). (b) A magification of the region $|\omega| < 0.04$ for $n_a = 0.7$, 0.8, 1.0, 1.2.

FIG. 5. The reduced concentration of adsorbed chains, $c_a(x)/c_{b0}$, in the slit of width h between 2 solid surfaces vs. the distance x to the nearest surface, $0 < x < h/2$, for $h/R_a = 0.6$, 1.4, 2.8, 3.8, 10 (top to bottom); $R_a = a\sqrt{N_a}$ is the Gaussian gyration radius of an adsorbed chain.

FIG. 6. The reduced interaction potential $\bar{W}$ vs. reduced separation $\bar{h} = h/R$ between the solid surfaces for $n_a = 1$, $X = 50$, 100, 200, 500 (from left to right) and $r_b = 0.1$ (a), $r_b = 0.9$ (b).

FIG. 7. The reduced potential $\bar{W}(\bar{h})$ for different $r_b = 0.1$, 0.2, 0.3, 0.4, 0.5, 0.6, 0.7, 0.8, 0.85, 0.9, 0.95, 0.98 (from left to right), $n_a = 1$, $X = 500$.

FIG. 8. The reduced interaction potential $\bar{W}/r_b^2$ vs. $\bar{h} = h/R$ for $n_a = 1$. The curves from left to right correspond to: (1) theory, eq. (41), for $r_b \ll 1$; (2-4) SCFT results for $r_b = 0.05$, 0.1, 0.2.

FIG. 9. (a) The reduced FPI interaction potential $\bar{W}$ vs. $\bar{h}$, calculated using the SCFT approach for different length of adsorbed polymer, $n_a = R_a/R =$ 0.1, 0.2, 1/3, 0.5 (dashed curves), 4/7, 2/3, 0.8, 1 (solid curves from left to right). $r_b = 1$ and $X = 500$ in all the cases. The leftmost solid curve corresponds to purely repulsive surfaces and no adsorbed layer, that is to $n_a = 0$ (see the text). (b) The same data zoomed in.

FIG. 10. (a) The depth of the attraction well, $|\bar{W}_{min}|$, as a function of n_a. (b) The height of the distal (secondary) repulsion barrier, $\bar{W}_2^*$, as a function of n_a (the dashed line comes from part (a) for comparison).

FIG. 11. The n_a-dependence of the positions of the attraction well, $\bar{h}_{min}$ (solid curve) and the distal barrier, $\bar{h}_2^*$ (dashed).

FIG. 12. The FPI interaction potential $U(h)$ vs. h/R: (a) The SCFT results for $\varkappa \gg 1$, $A_R = 80$, $r_b = 1$ and $n_a = 1$, 0.8, 0.67, 0.57 (from right to left). $U(h)$ was calculated based on the data shown in figure 9. (b) Analytical results obtained using eq. (44) for $\varkappa \ll 1$, $\varkappa^2 A_R = 10$ and $n_a = 1$, 0.8, 0.7, 0.6 (from right to left). The inset shows a blow-up of the region $1.5 < h/R < 4$.

FIG. 13. The total interaction potential $U_{tot}(h) = U(h) + U_H(h)$ vs. h/R for $D_c = 200$nm, $R \approx 3$nm, $A_H = 1\ k_BT$ and $U(h)$ for different $n_a = 0.57$, 0.67, 0.8, 1 (from left to right) corresponding to the data shown in Fig. 12(a).

FIG. 14. The dependence of the reduced polymer-induced interaction potential between spherical particles U_{FPI}/A_R on their separation h for $h > h^*$. (a) $\xi/R = 0.125$, $\varkappa = 0.25$, 0.3, 0.4, 0.5 (from bottom to top). (b) $\varkappa = 0.5$, $\xi/R = 0.15$, 0.2, 0.25, 0.3 (from top to bottom). All the potential curves are calculated using eqs. (49), (33), (50).

FIG. 15. The region of colloidal stability (where the FPI repulsion dominates) is located above the critical line in the c_b, N plane. The characteristic concentration and polymerization index are $c_1 \sim (\sigma_a/a)^{2/3} / (v^*)^{1/3}$, $N_1 \sim \left(\frac{a}{\sigma_a v^*}\right)^{2/3}$; $c_{max} = 1/v_1$.

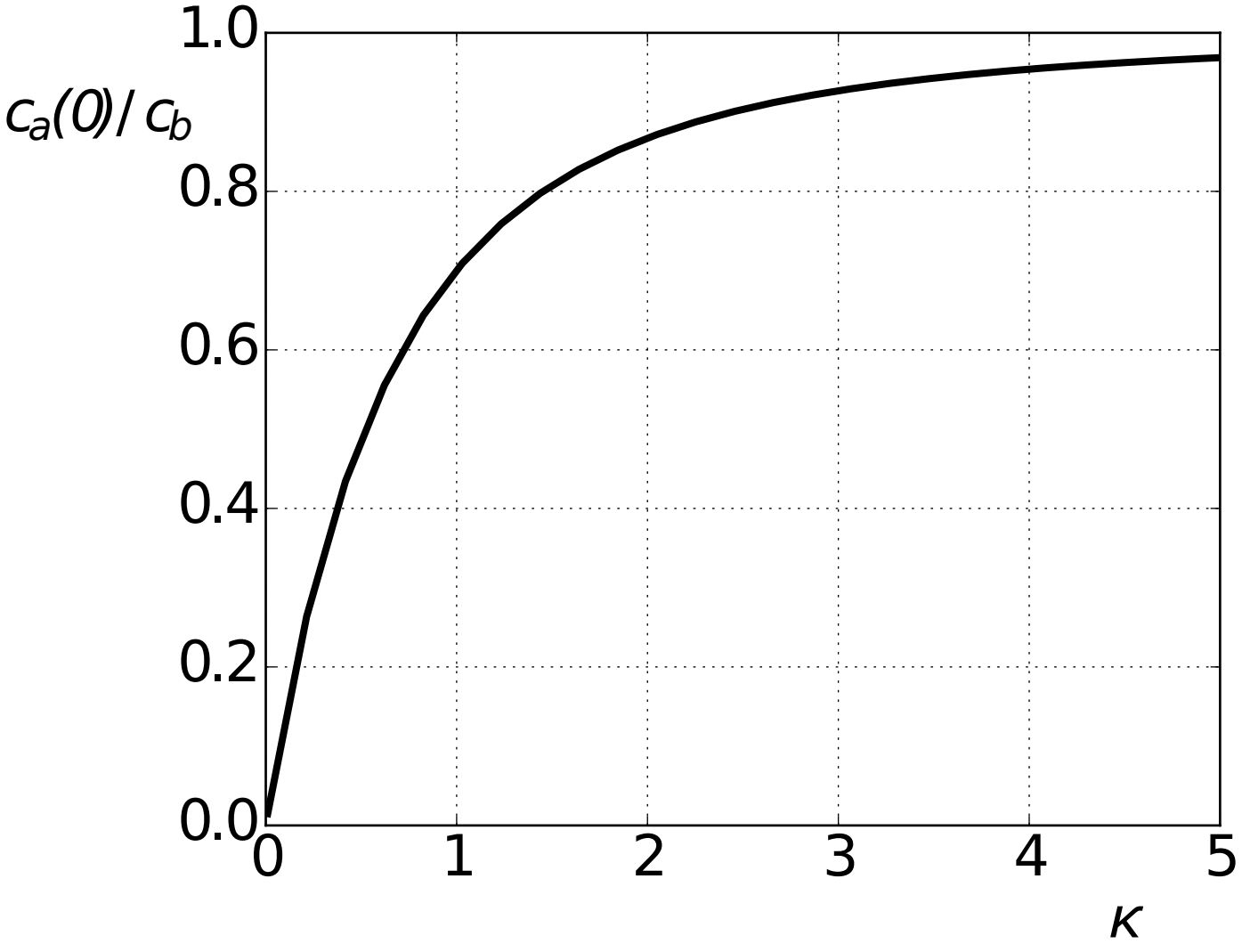

Fig. 1

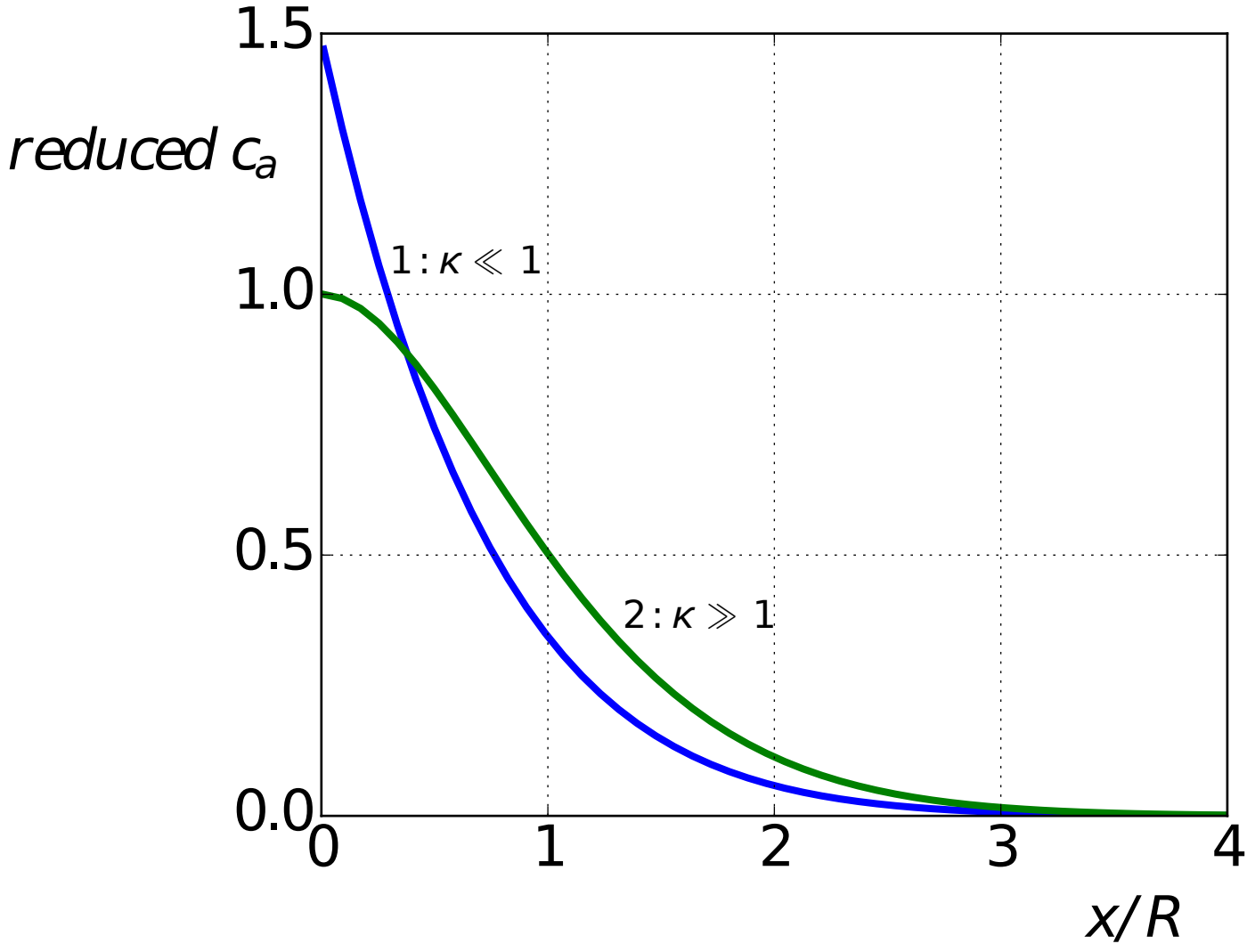

Fig. 2

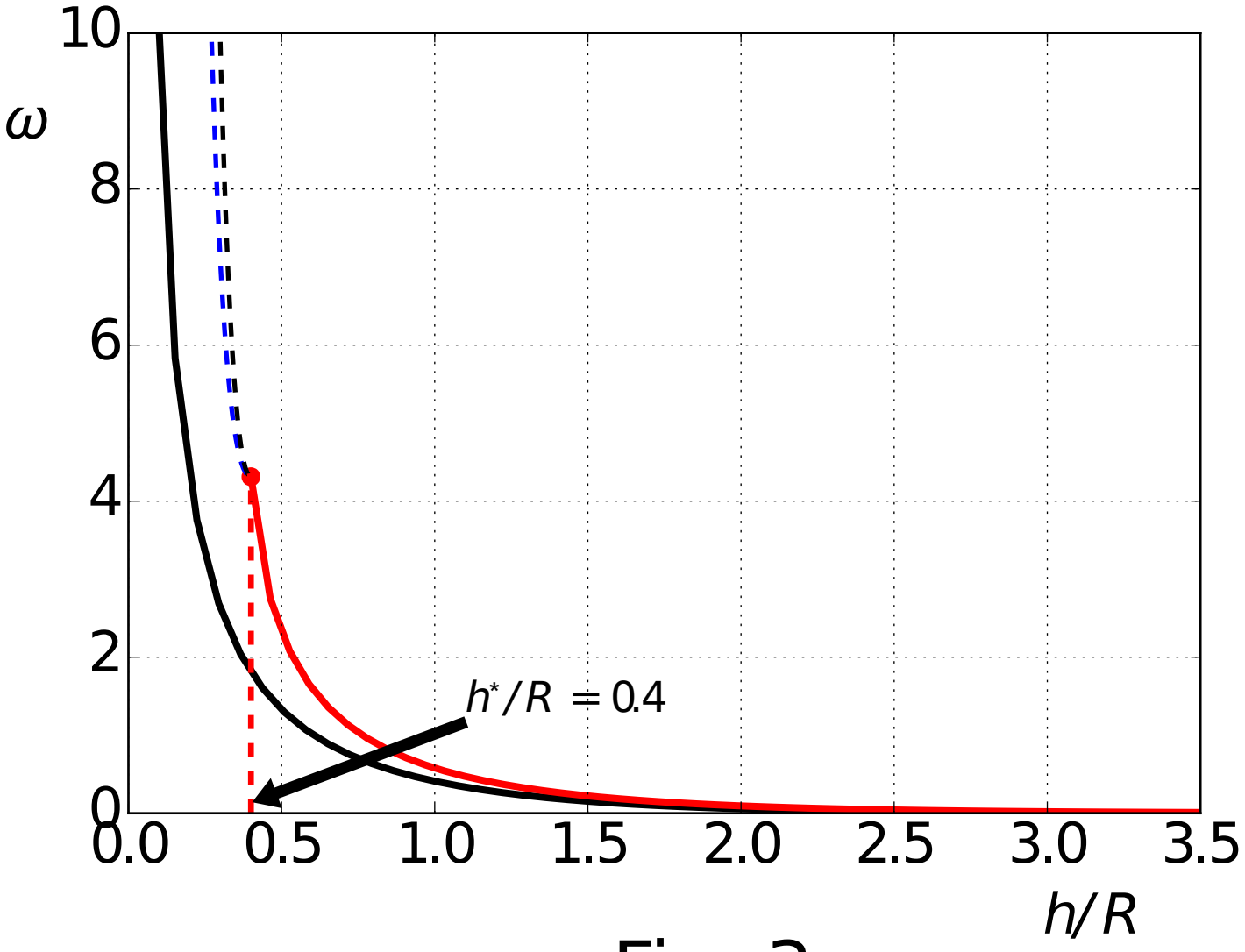

Fig. 3

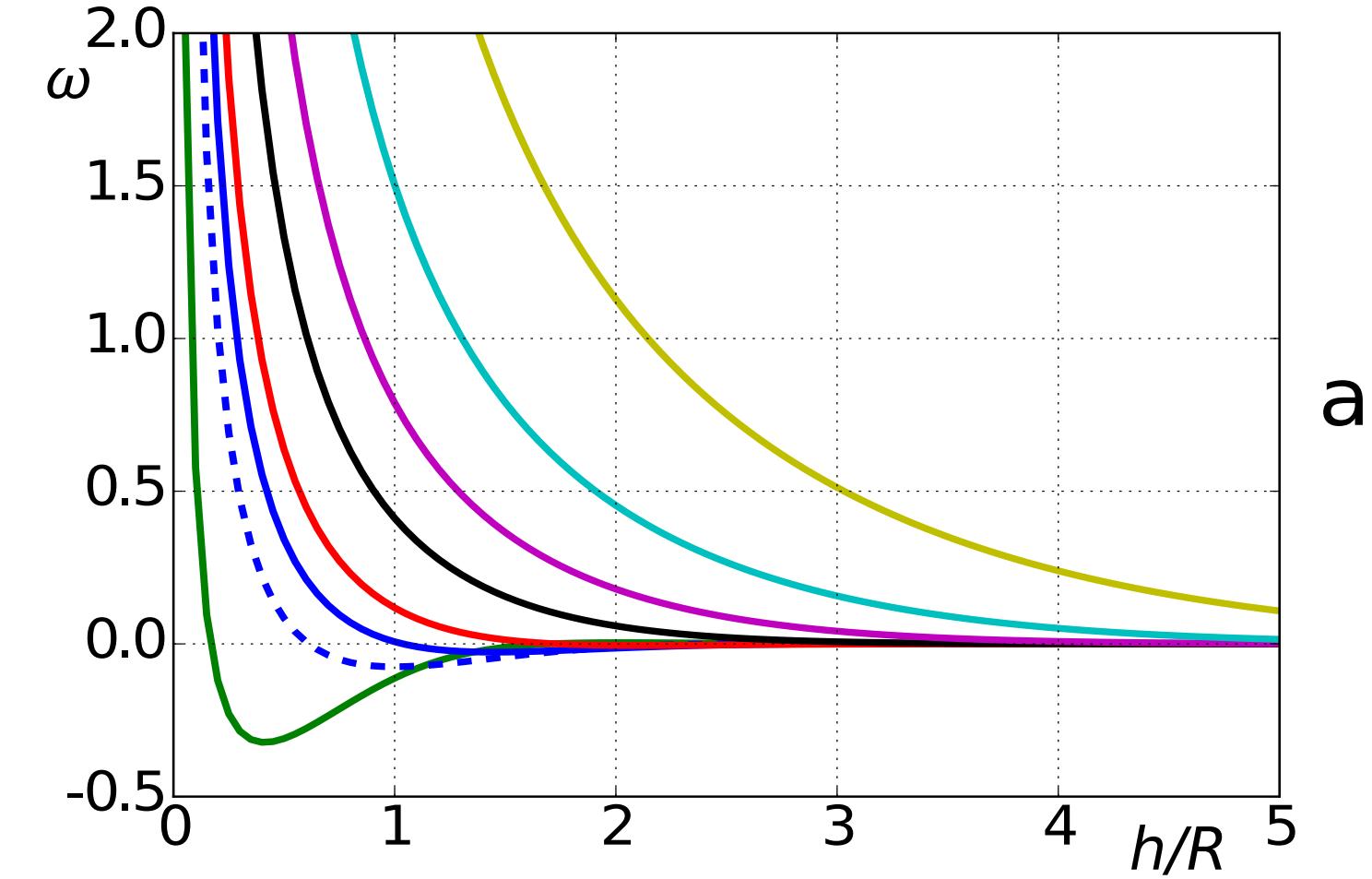

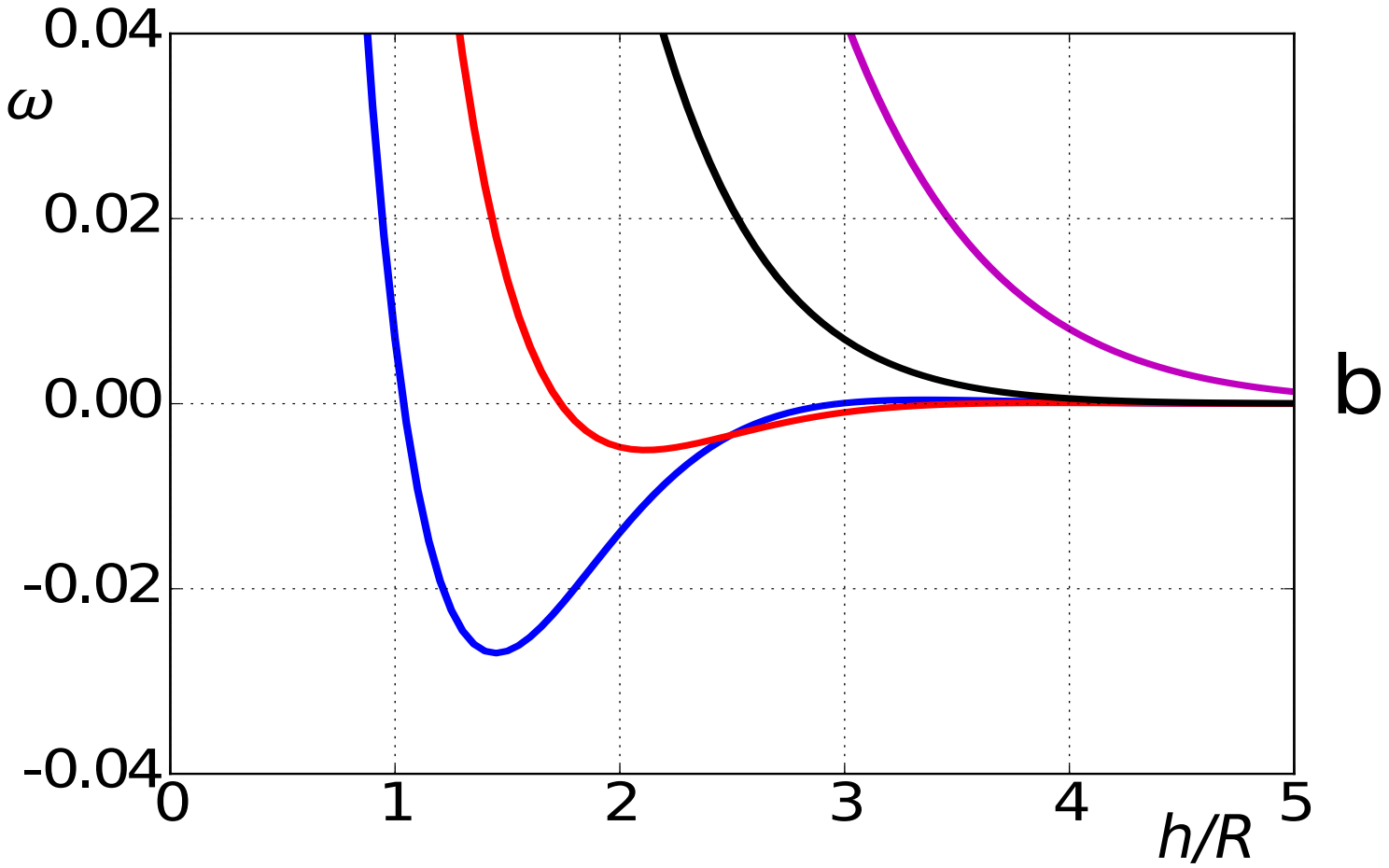

Fig. 4

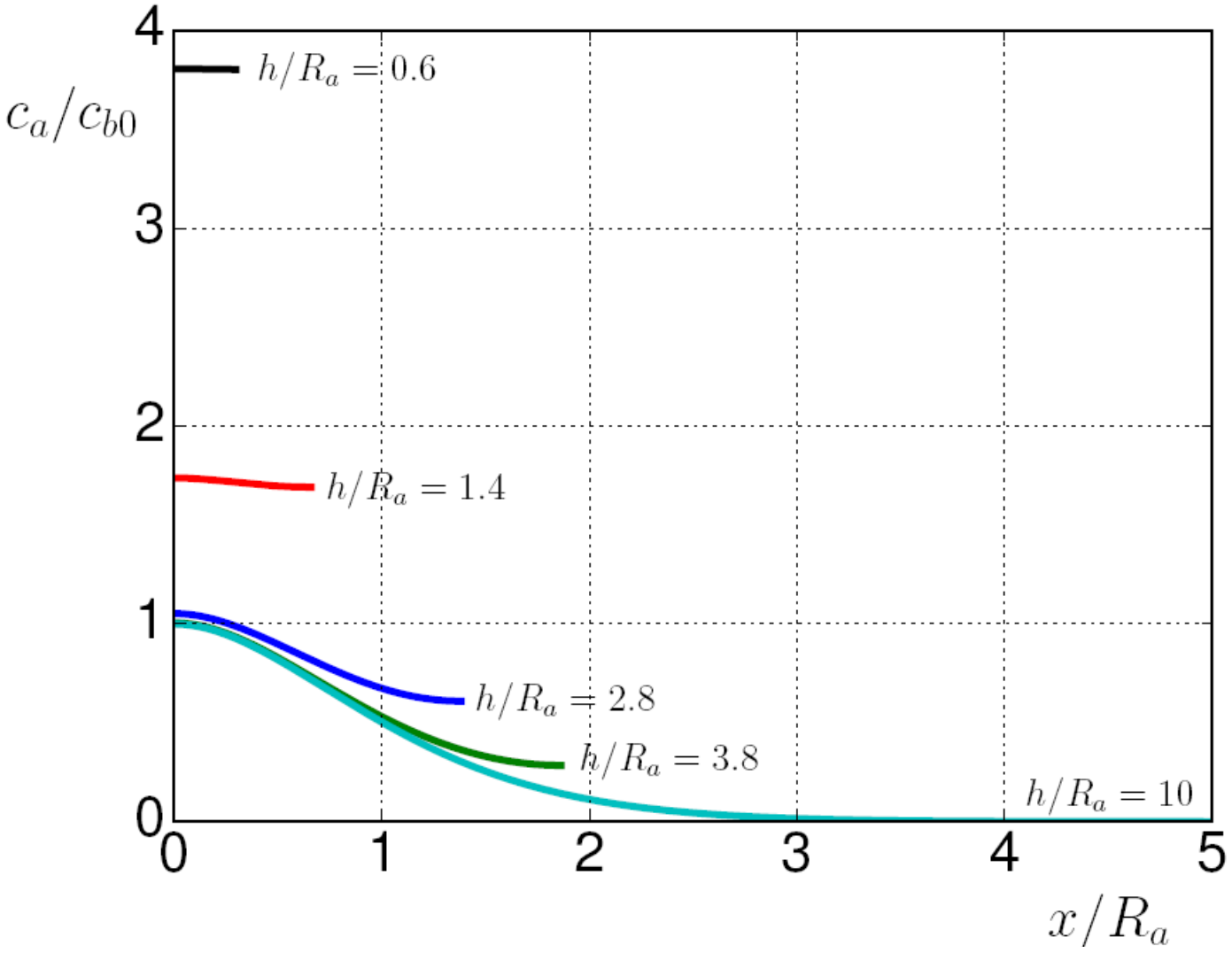

Fig. 5

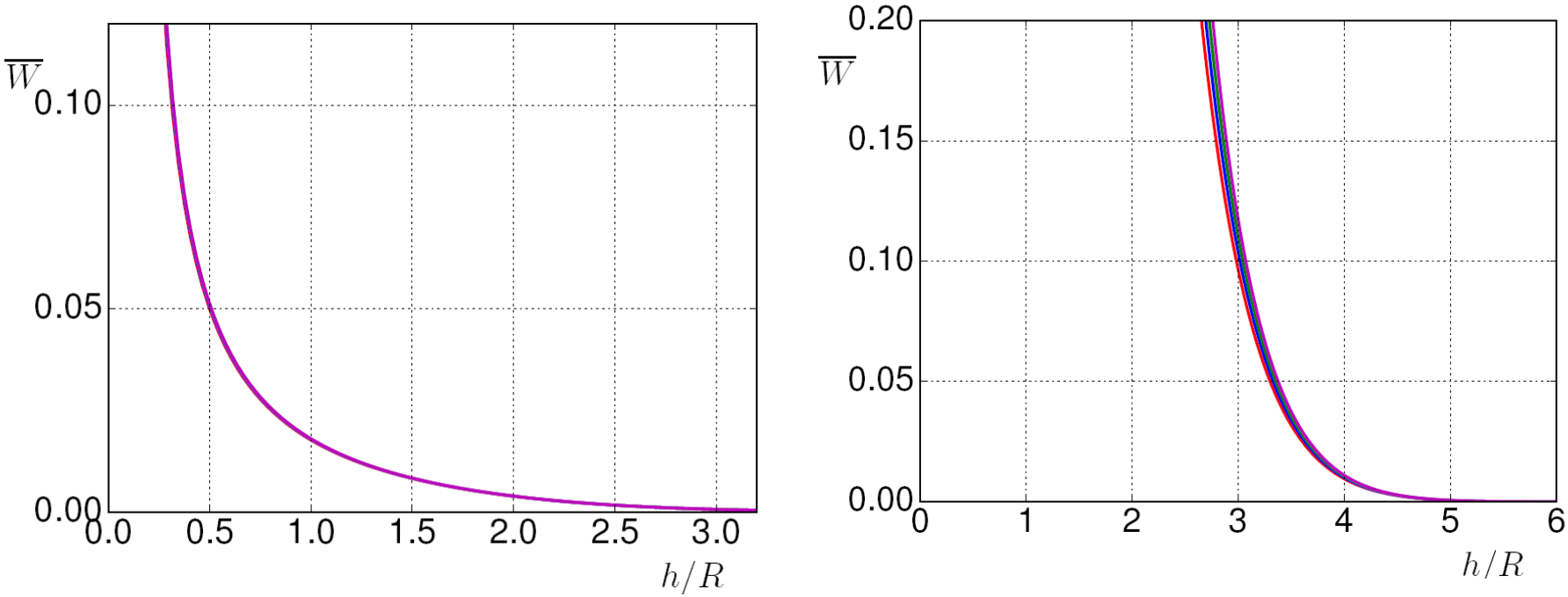
$\overline{W}$
0.10
0.05
0.00
0.0
0.5
1.0
1.5
2.0
2.5
3.0
h/R
$\overline{W}$
0.20
0.15
0.10
0.05
0.00
0
1
2
3
4
5
6
h/R

(a) (b)

Fig. 6

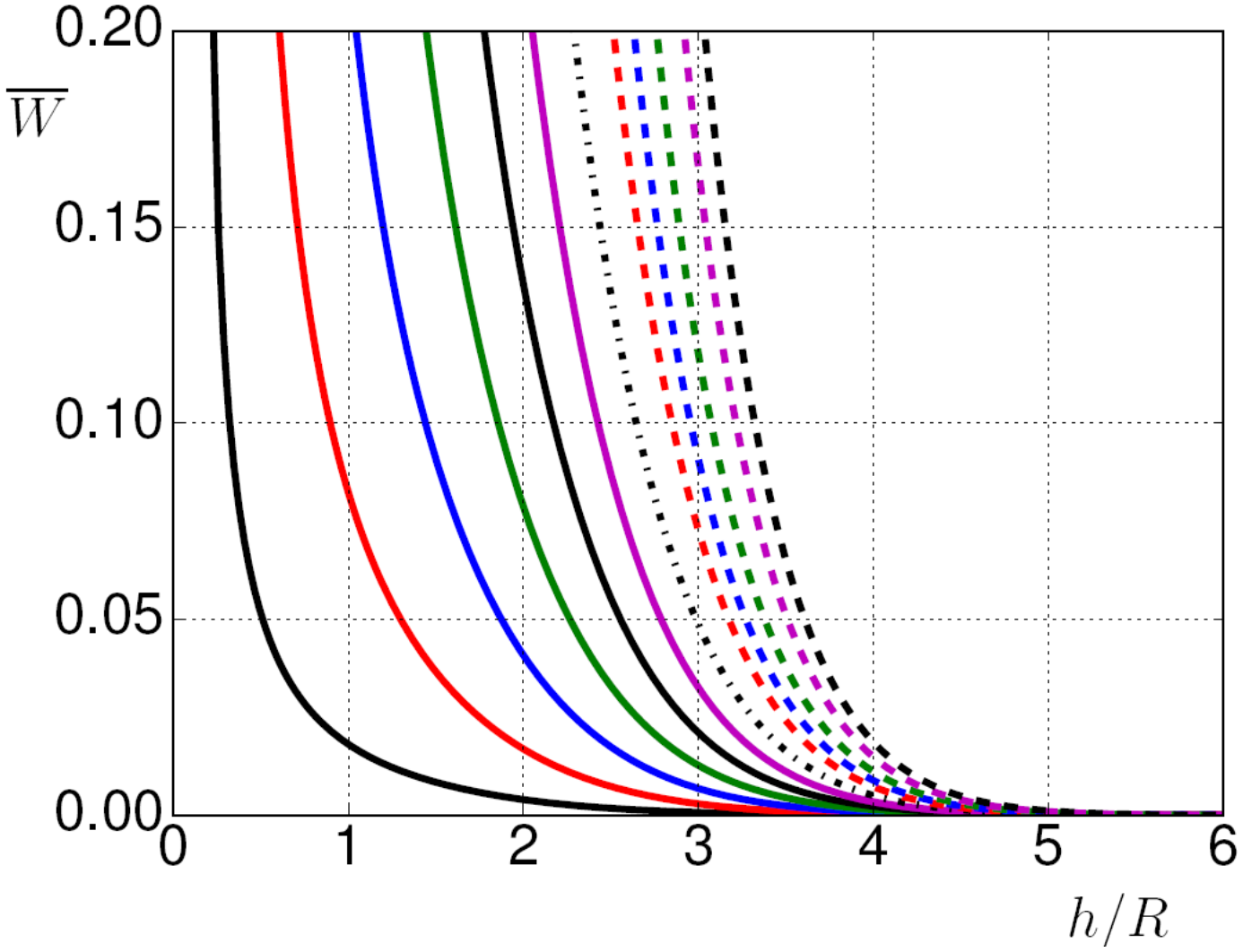

Fig. 7

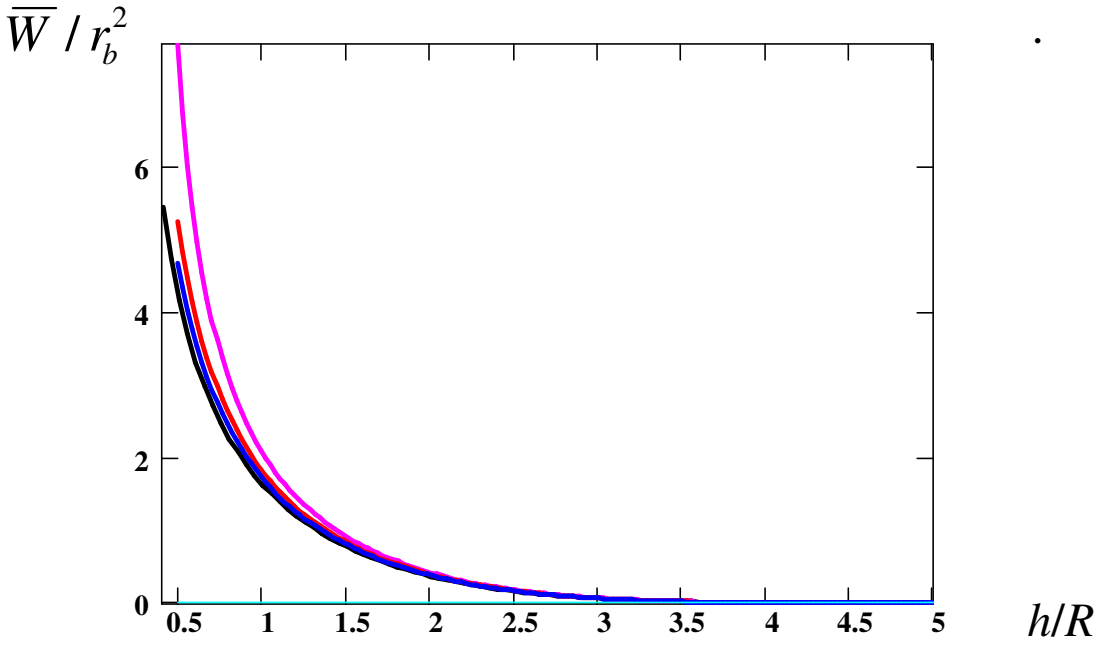

Fig. 8

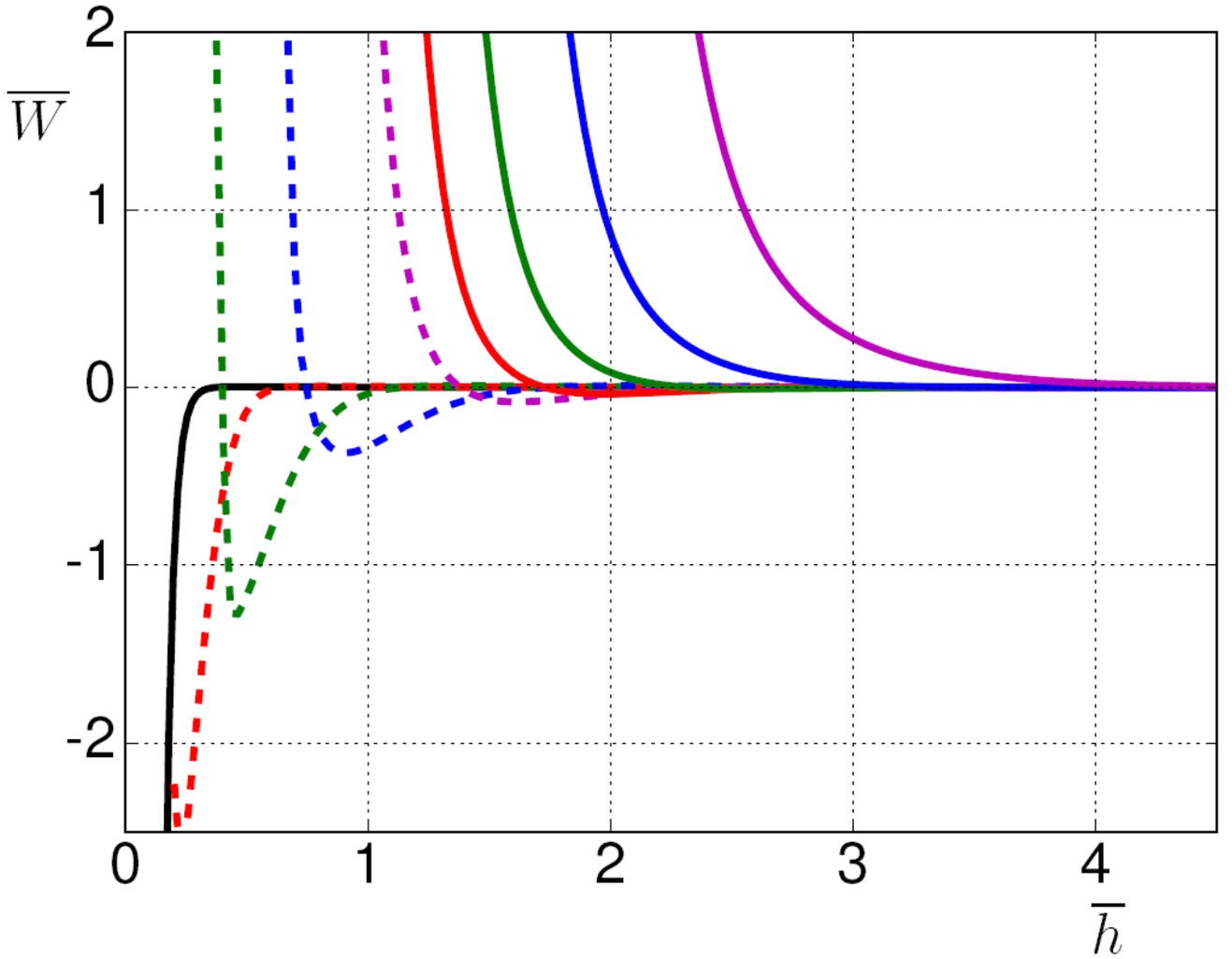
$\overline{W}$
2
1
0
-1
-2
0
1
2
3
4
$\overline{h}$

(a)

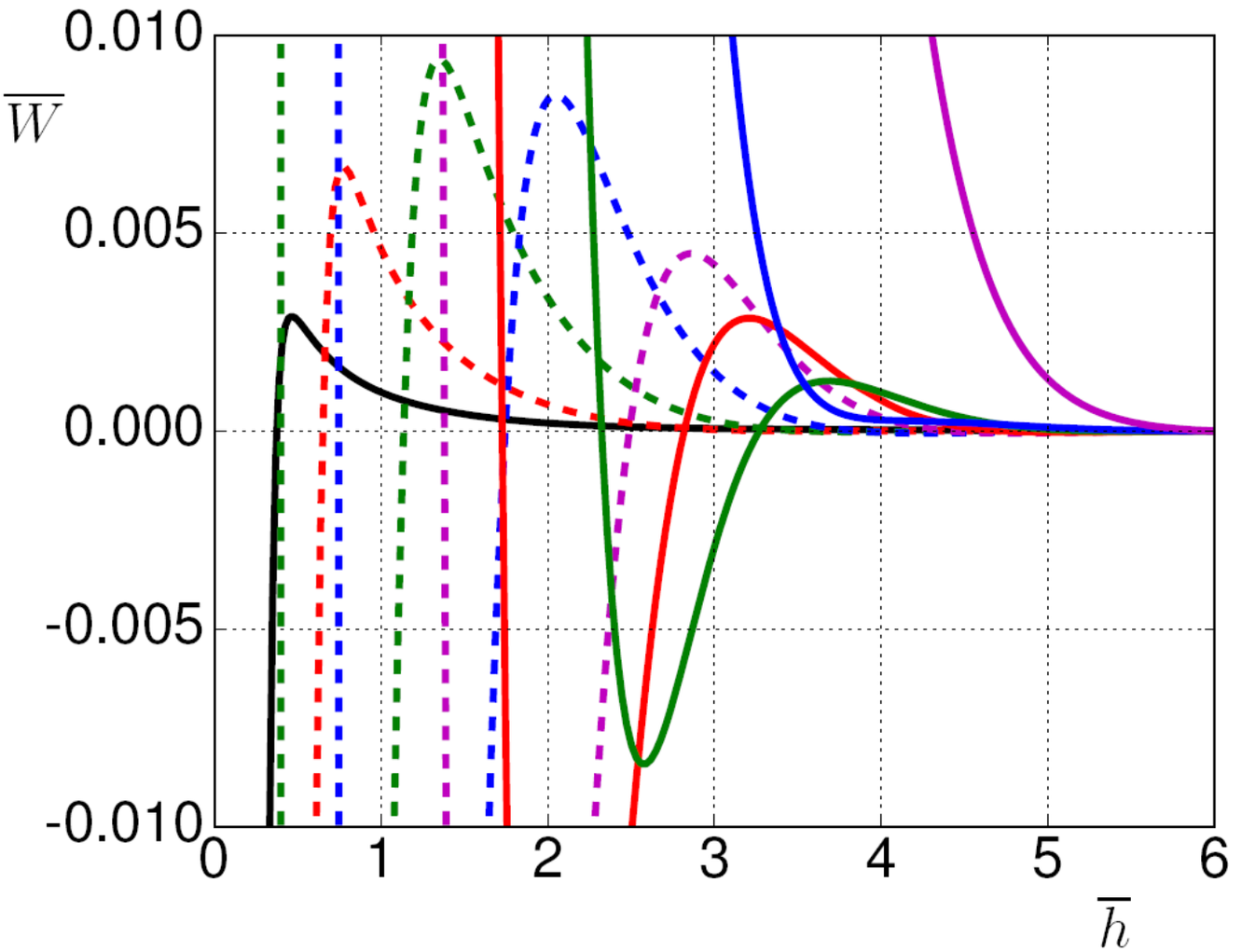
$\overline{W}$
0.010
0.005
0.000
-0.005
-0.010
0
1
2
3
4
5
6
$\overline{h}$

(b)

Fig. 9

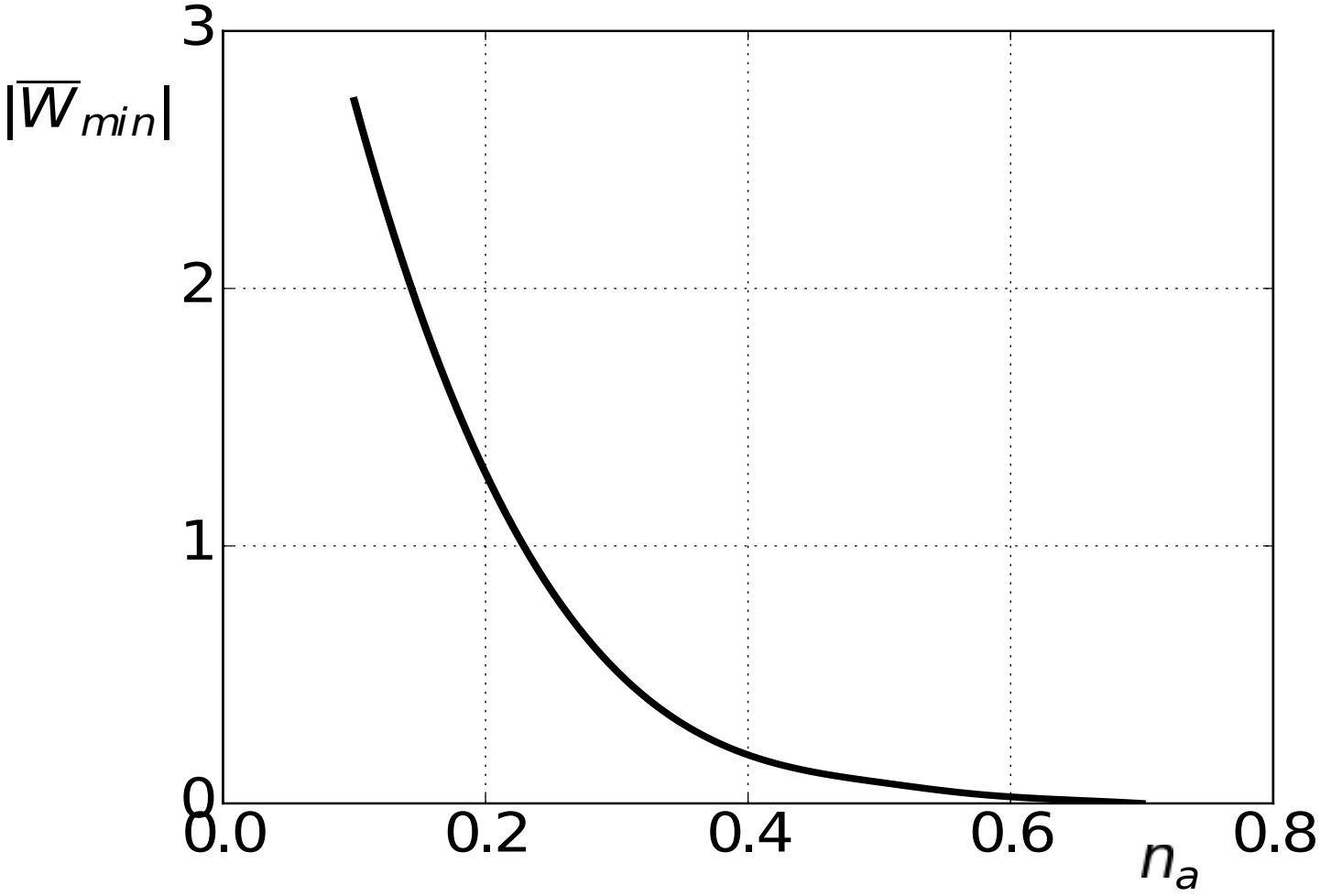
$|\overline{W}_{min}|$
3
2
1
0
0.0
0.2
0.4
0.6
0.8
n_a

a

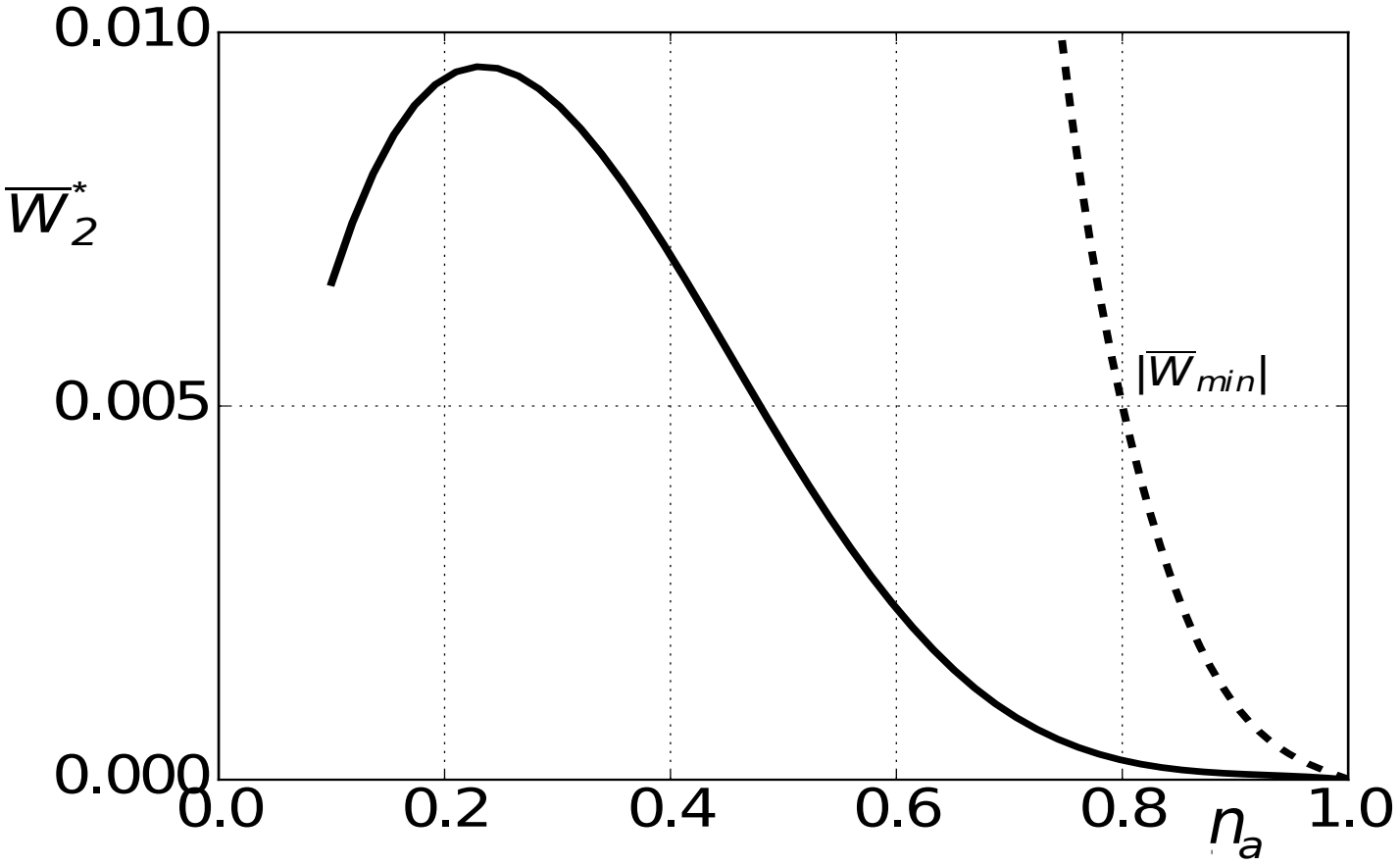
$\overline{W}_2^*$
0.010
0.005
0.000
$|\overline{W}_{min}|$
0.0
0.2
0.4
0.6
0.8
1.0
n_a

b

Fig. 10

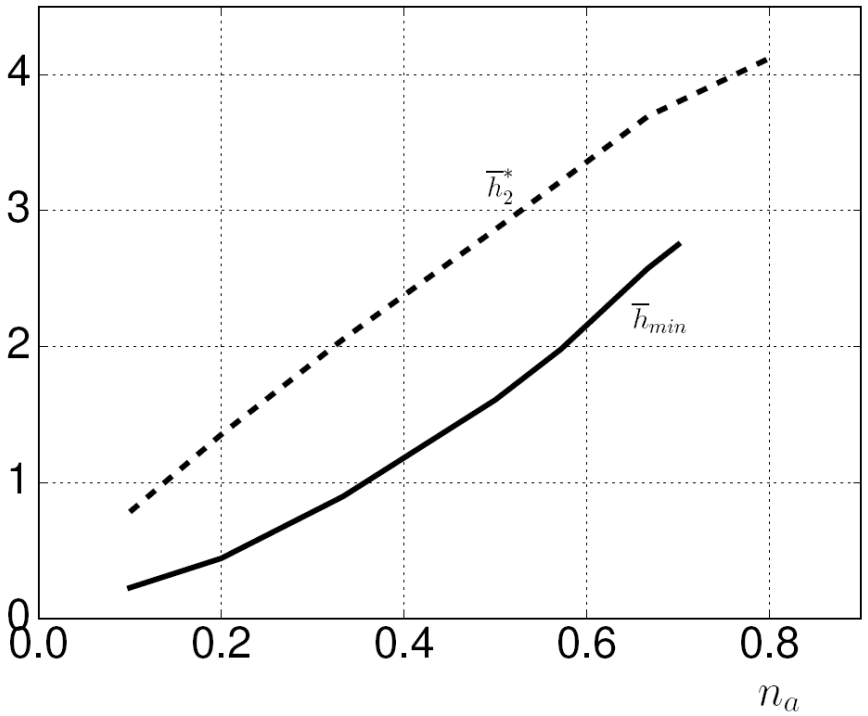

Fig. 11

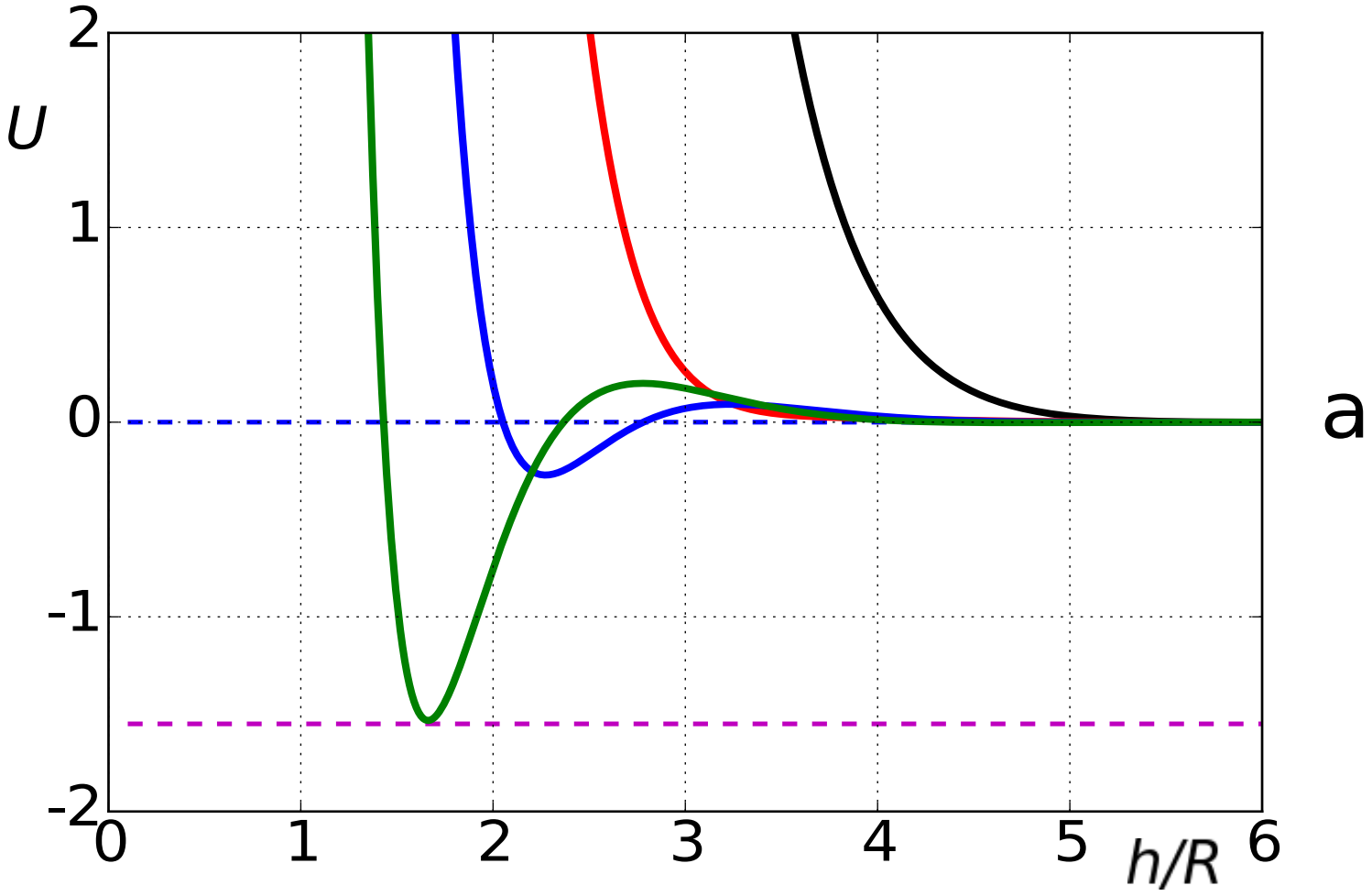

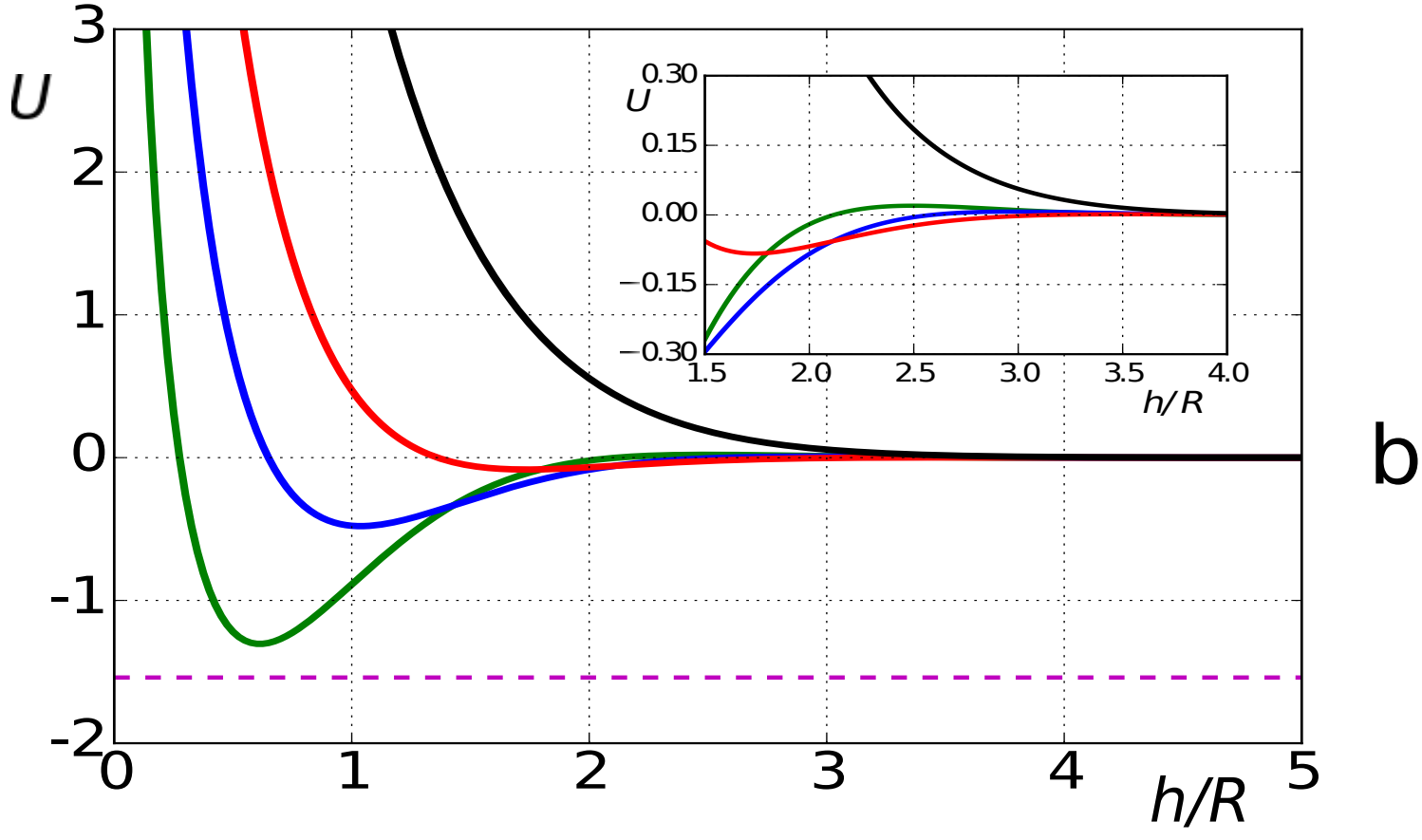

Fig. 12

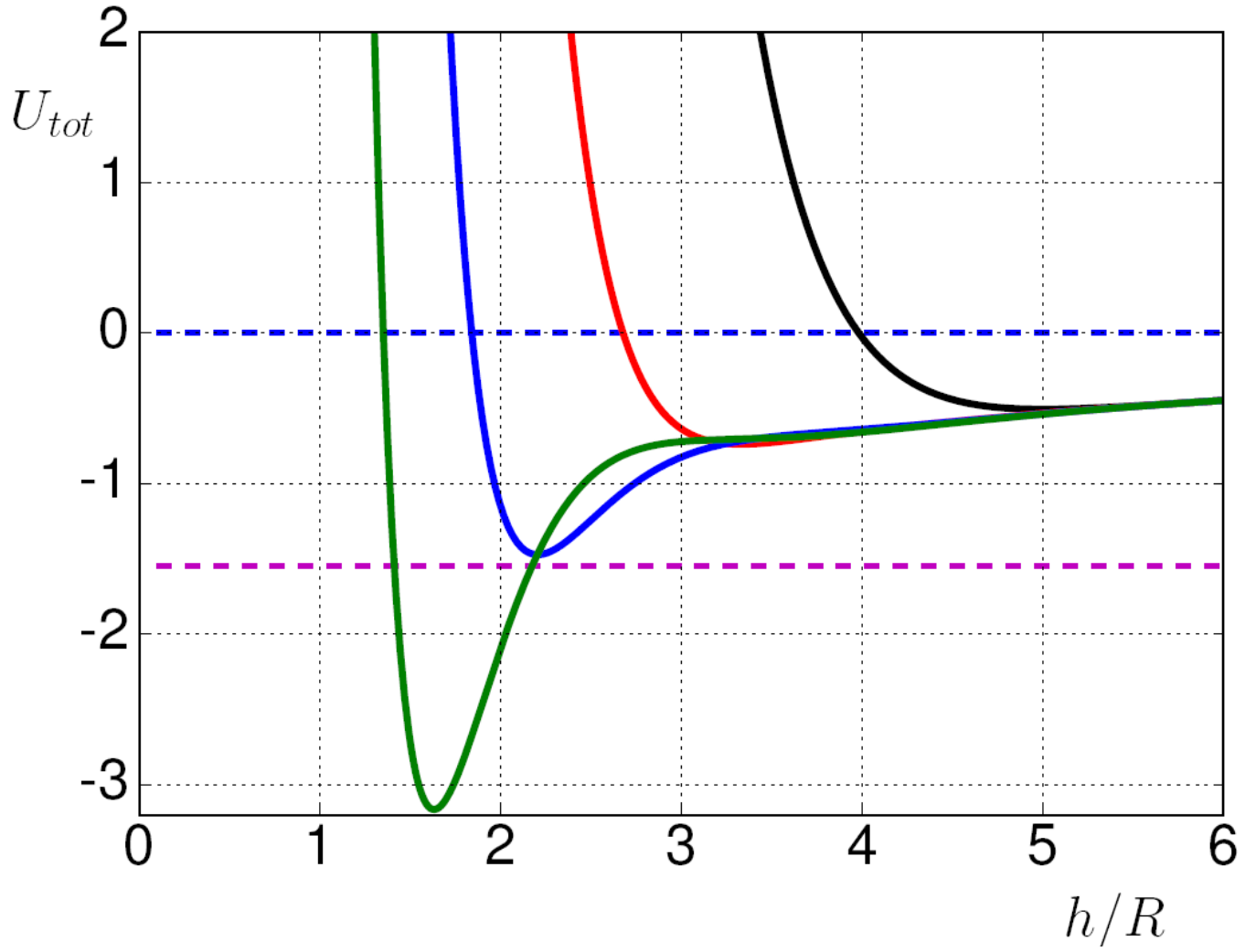

Fig. 13

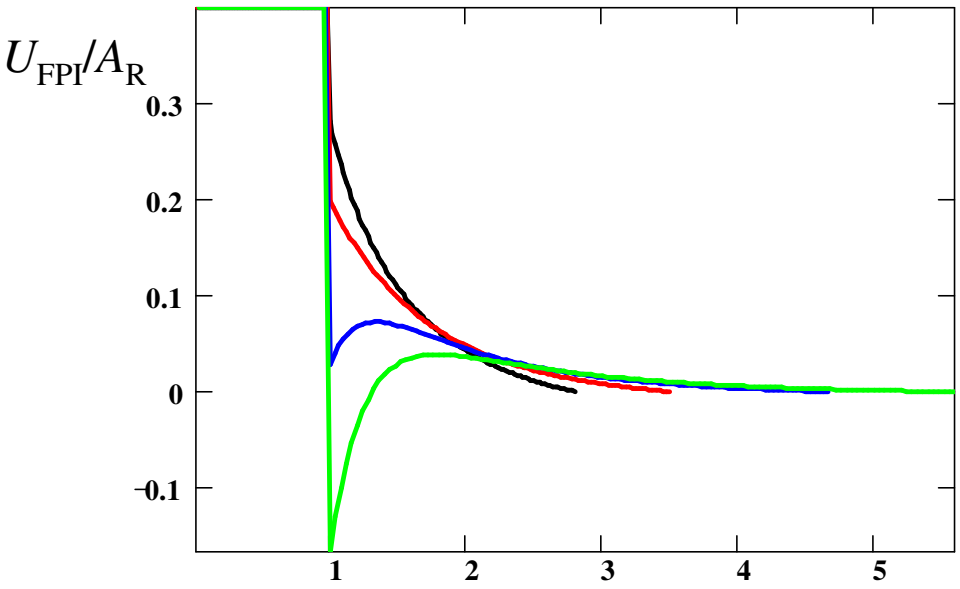

(a)

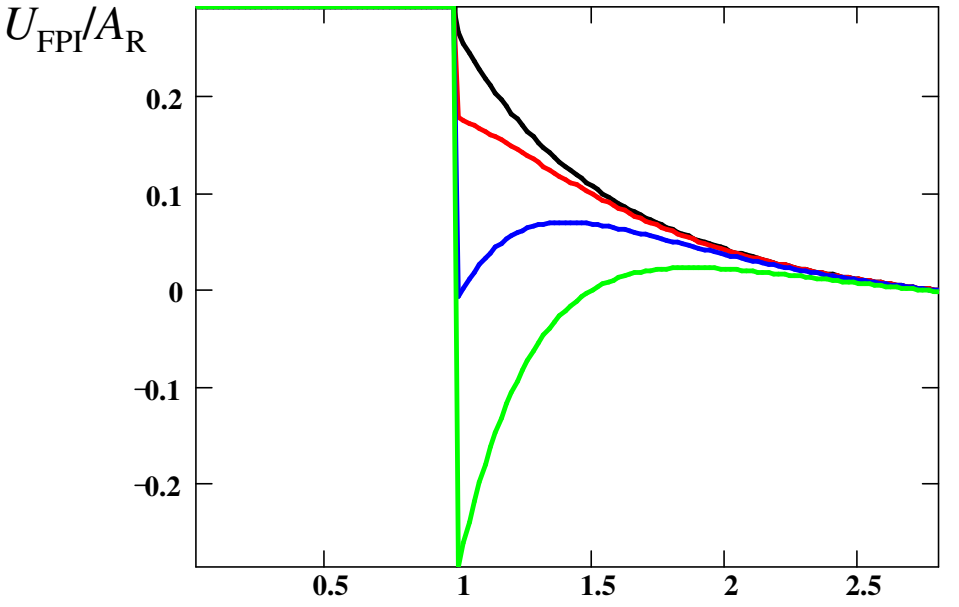

(b)

Fig. 14

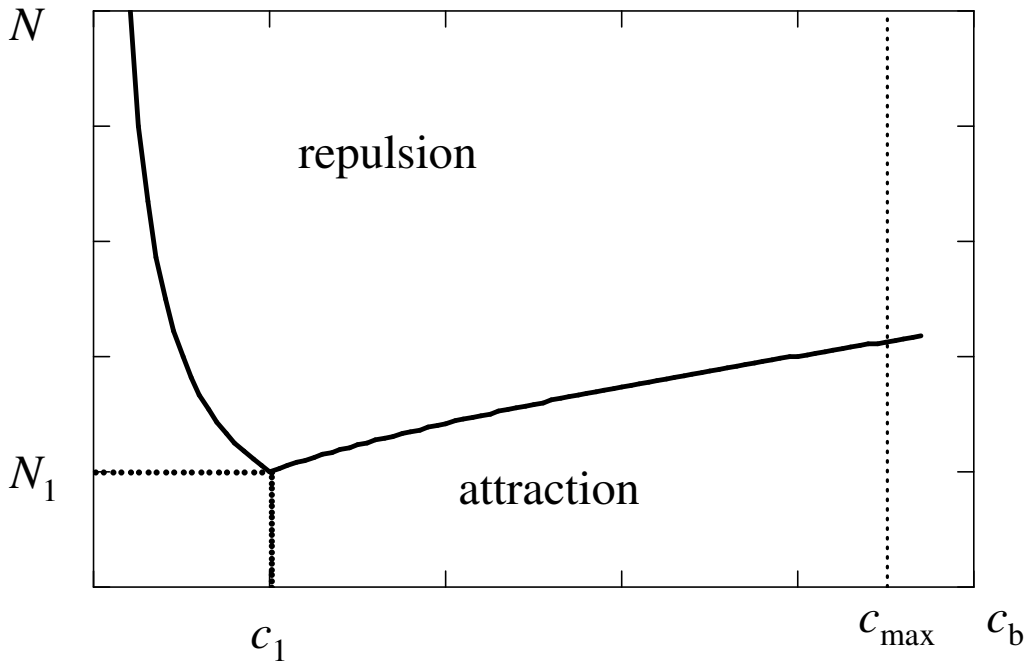

Fig. 15